Contributions to Mineralogy and Petrology (2019) 174:43
https://doi.org/10.1007/s00410-019-1580-8

ORIGINAL PAPER

Signature of deep mantle melting in South Iceland olivine

Paavo Nikkola[1,2] · Guðmundur H. Guðfinnsson[2] · Enikő Bali[2,3] · O. Tapani Rämö[1] · Tobias Fusswinkel[4] · Thorvaldur Thordarson[2,3]

Received: 1 December 2018 / Accepted: 26 April 2019 / Published online: 13 May 2019

Abstract

We present new high-precision major and trace element data on olivine macrocrysts from various volcano-tectonic settings in Iceland and use these data as a proxy for mantle mode and melting conditions. Within individual sampling sites examined (seven lavas and one tephra) olivine-dominated fractional crystallization, magma mixing and diffusive re-equilibration control observed variability in olivine composition. High-pressure fractional crystallization of clinopyroxene may have lowered Ca and increased Fe/Mn in one olivine population and subsolidus diffusion of Ni and Fe–Mg affected the mantle-derived Ni/Fo ratio in some compositionally zoned olivine macrocrysts. Interestingly, magmas erupted at the southern tip of the Eastern Volcanic Zone (SEVZ), South Iceland, have olivines with elevated Ni and low Mn and Ca contents compared to olivines from elsewhere in Iceland, and some of the SEVZ olivines have relatively low Sc and V and high Cr, Ti, Zn, Cu and Li in comparison to depleted Iceland rift tholeiite. In these olivines, the high Ni and low Mn indicate relatively deep melting ($P_{\text{final}} > 1.4$ GPa, ~ 45 km), Sc, Ti and V are compatible with low-degree melts of lherzolite mantle, and elevated Zn may suggest modal (low-olivine) or geochemical (high Zn) enrichment in the source. The SEVZ olivine macrocrysts probably crystallized from magmas derived from olivine-bearing but relatively deep, enriched and fertile parts of the sub-Icelandic mantle, and indicate swift ascent of magma through the SEVZ lithosphere.

Keywords Olivine · Trace elements · Mantle heterogeneity · Mantle melting · Iceland

Introduction

Icelandic mantle

Although many of the details remain obscure, Earth's mantle is evidently heterogeneous in mineralogy and chemical composition (Allègre and Turcotte 1986). A major source of this heterogeneity is subducted oceanic crust that contributes to the mantle source of oceanic island basalts (Hofmann and White 1982; Hauri 1996; Chauvel et al. 2008). In Iceland, there is abundant isotopic evidence for recycled oceanic crustal material in the upper mantle (Fitton et al. 1997; Chauvel and Hémond 2000; Kokfelt et al. 2006; Peate et al. 2010). Anyhow, isotope systematics do not yield straightforward information about mantle lithology, and it is yet unclear whether the recycled oceanic crust resides in the mantle as a discrete rock type, i.e. pyroxenite or eclogite, or if it has been completely mixed with the dominant mantle peridotite (Green and Ringwood 1963).

Insights into the modal composition of the mantle can be acquired by studying the major and trace element

Communicated by Mark S Ghiorso.

Electronic supplementary material The online version of this article (https://doi.org/10.1007/s00410-019-1580-8) contains supplementary material, which is available to authorized users.

✉ Paavo Nikkola
paavo.nikkola@helsinki.fi

[1] Department of Geosciences and Geography, Geology and Geophysics Research Group, University of Helsinki, P. O. Box 64, 00014 Helsinki, Finland

[2] Nordic Volcanological Center, Institute of Earth Sciences, Sturlugata 7, 101 Reykjavík, Iceland

[3] Faculty of Earth Sciences, University of Iceland, Sturlugata 7, 101 Reykjavík, Iceland

[4] Institute of Applied Mineralogy and Economic Geology, RWTH Aachen University, Wüllnerstr. 2, 52062 Aachen, Germany

composition of magmas that represent partial melts of the mantle. This is, however, prone to uncertainty, as the nature of mantle melts is dependent on not only the modal composition of the mantle but also melting temperature (T), pressure (P) and the degree of melting (F). In addition, mantle-derived magmas are usually modified in the crust by low-P fractional crystallization, magma mixing and crustal contamination, which may obscure the traits they inherited from the source. Nevertheless, with careful treatment of the data, the quantity of possible end-member mantle source rock-types can be estimated, and the inferred mantle components can be further assessed by comparing their assumed melt productivity to crustal thickness (Shorttle and Maclennan 2011; Brown and Lesher 2014; Shorttle et al. 2014; Lambart 2017). Using this approach, it has been established that melting of depleted lherzolite alone is unlikely to produce the compositional variability (especially the high Fe and low Ca) in Icelandic lavas (Shorttle and Maclennan 2011). A minor (4–15%) olivine-free pyroxenite or mixed pyroxenite–peridotite hybrid seem to be required in the mantle source (Shorttle et al. 2014).

Besides utilizing the major and trace element composition of magmas, the nature of the mantle source can be probed by analyzing forsteritic olivine macrocrysts. The composition of forsteritic olivine reflects the composition of its near-primary parental magma, and hence the mode (Sobolev et al. 2005) and/or melting conditions (Li and Ripley 2010; Matzen et al. 2013, 2017a, b) in the mantle source. In Iceland, olivine compositions have been found to be rather consistent with shallow melting of lherzolite (Herzberg et al. 2016), although some lavas have olivines with higher Ni than expected by models of fractional crystallization of peridotite-derived melts (Shorttle and Maclennan 2011; Herzberg et al. 2016; Neave et al. 2018). These Ni-rich olivines have been suggested to indicate melting of enriched, olivine-free or olivine-poor, mantle below Iceland (Sobolev et al. 2007, 2008; Shorttle and Maclennan 2011), or explained by mixing of variably differentiated lherzolite-derived melts in the crust (Herzberg et al. 2016).

We present new olivine trace element data from various volcano-tectonic settings in Iceland, gathered using high probe current microprobe and laser ablation inductively coupled plasma mass spectrometry (LA–ICP–MS) methods. The primary finding are the relatively Ni-enriched and Mn- and Ca-poor olivine macrocrysts from Eyjafjallajökull and Vestmannaeyjar volcanic systems, exceptional in the context of pre-existing data (Sobolev et al. 2007; Shorttle and Maclennan 2011; Neave et al. 2018). Some of these olivine crystals are also enriched in Ti, Zn, Cu, Li, Cr and depleted in Sc and V compared to olivines from rift zone tholeiite (Háleyjabunga). We propose that the parental magma of these olivine macrocrysts equilibrated at high temperatures and pressures with a fertile olivine-bearing mantle source.

Olivine as indicator of mantle mode and melting conditions

In mantle lherzolite, abundant residual olivine limits the Ni content of partial melts by effectively sequestering Ni. In contrast, low-degree partial melts of olivine-free pyroxenite are, in most cases, rich in Ni, and poor in Mn and Ca as garnet and clinopyroxene in the residuum preferentially sequester Mn and Ca, but not Ni. Ni, Mn and Ca are stored in early-formed Fo-rich olivine in proportion to their content in primitive melts, even if the melt is later modified by fractional crystallization and magma mixing. Because of this, trace elements in olivine should record the lithology of the mantle source. Sobolev et al. (2005) were the first to use high-Ni, low-Mn and low-Ca in olivine as an indicator of olivine-free pyroxenite in the mantle. Since this work, olivine composition has been used to estimate the mantle lithology for a wide range of volcanic provinces (e.g. Sobolev et al. 2007, 2008; Herzberg 2011; Herzberg et al. 2014; Trela et al. 2015).

Using olivine as a mantle proxy is complicated by variation in T, P, and oxygen fugacity (fO_2) that affects element partitioning in mantle melting and subsequent olivine crystallization. Recent experimental work suggests that Ni and Mn distribution coefficients between olivine and melt ($D_{Ni}^{ol/liq}$, $D_{Mn}^{ol/liq}$) are, directly or indirectly, dependent on temperature of mantle melting (Li and Ripley 2010; Putirka et al. 2011; Matzen et al. 2013, 2017a, b). $D_{Ni}^{ol/liq}$ is relatively low for high-temperature peridotite melting at high pressures, which results in partial melts relatively enriched in Ni. Consequently, when a deep mantle-derived magma rises to a lower temperature and pressure environment, $D_{Ni}^{ol/liq}$ is higher, resulting in crystallization of Ni-rich olivine (Matzen et al. 2013, 2017a). $D_{Mn}^{ol/liq}$ correlates positively with MgO in the melt, and MgO-rich melts of peridotite are generated at higher temperature; therefore, high-temperature mantle melts have lower MnO and they crystallize low-Mn olivine macrocrysts (Matzen et al. 2017b). This, and the global correlation between lithospheric thickness and olivine compositions, has sparked a debate on whether the variation in Ni and Mn in olivines reflect the depth of mantle melting or variation in mantle mode (Niu et al. 2011; Heinonen and Fusswinkel 2017; Putirka et al. 2018). Mn partitioning between partial melts and mantle residue may also be susceptible to water content in the mantle (Balta et al. 2011), and the extent of parental melt polymerization (NBO/T) has been proposed to affect Ni partitioning during olivine crystallization (Wang and Gaetani 2008). Also, the slower diffusion of

Ni compared to Mg and Fe in olivine lattice during crustal storage can affect element ratios in zoned olivine (Lynn et al. 2017).

Because complexly influenced by parameters of melting and crystallization, olivine compositions need not to be directly related to the volume of a certain rock type in the mantle, e.g. olivine-free pyroxenite. Nevertheless, olivine macrocrysts are useful, as their composition echoes the evolutionary history of an individual melt, i.e. they record fractional crystallization and magma mixing, and the most primitive olivines in a system mirror the composition of the original mantle-derived melt in a way glass or whole-rock composition of magmas nearly never do. Olivine composition is a high-detail mantle proxy, valuable when treated in view of other mantle source indicators, such as major, trace element and isotopic composition of magmas.

Sampling and geological background

Sample locations

We analyzed olivines from eight locations, which represent varying volcano-tectonic environments in Iceland. These include Háleyjabunga and Mosfellsheiði lavas in southwestern Iceland; Kistufell hyaloclastite in the central highlands; Berserkjahraun lava of the Snæfellsnes Volcanic Zone (SVZ); and Stórhöfði, Hvammsmúli, Brattaskjól lavas and Eyjafjallajökull 2010 summit tephra from the southern tip of the Eastern Volcanic Zone (SEVZ, Table 1, Fig. 1). The majority of olivine trace element data gathered earlier from Iceland are from the neovolcanic lavas of SVZ and the Northern Rift Zone (Sobolev et al. 2007, 2008). To gain new insights, we focused our sampling efforts on SEVZ (Fig. 1), where high-precision olivine analyzes had not been done earlier. Olivine major and trace element compositions from Háleyjabunga and Kistufell have been presented by Sobolev et al. (2007), and Háleyjabunga has also been revisited by Shorttle and Maclennan (2011) and Neave et al. (2018). Háleyjabunga and Kistufell are the end-members in terms of Ni and Mn content in the earlier Sobolev et al. (2007) high-precision data set from Iceland, and we re-analyzed them for assessment of data quality (cf. Supplementary Material).

Olivines from rift-zone tholeiites

The sampling locations Háleyjabunga, Mosfellsheiði and Kistufell represent the central parts of the mid-oceanic rift that lies across Iceland (Fig. 1); here the amount of decompression melting is generally the largest (Sæmundsson 1979). Háleyjabunga is a 13 ka (Sæmundsson 1995) lava shield situated near the tip of the Reykjanes Peninsula, known for its depleted isotopic and trace element character (Thirlwall et al. 2004). Our Háleyjabunga sample has the most magnesian olivines in our sample suite with forsterite (Fo) content up to 91 ($Fo = 100 \times$ atomic $Mg/(Mg + Fe^{2+})$). Mosfellsheiði is a younger than 700 ka (Sæmundsson et al. 2010) olivine-tholeiite lava flow field from the outskirts of

Table 1 The sample locations in this study with a collection of available geochemical data (Jakobsson 1979; Wiese 1992; Jóhannesson 1994; Breddam et al. 2000; Thirlwall et al. 2004, 2006; Peate et al. 2009, 2010; Sæmundsson et al. 2010; Sigmarsson et al. 2011)

	Rift-zones			SVZ	SEVZ			
	Háleyjabunga	Mosfellsheiði	Kistufell	Berserkjahraun	Hvammsmúli	Brattaskjól	Eyjafjallajökull 2010	Stórhöfði
Rock type[a]	Olivine tholeiite	Olivine tholeiite	Olivine tholeiite	Alkali basalt	Transitional basalt	Transitional basalt	Benmoreite/basalt[b]	Alkali basalt
Volcanic zone	WVZ	WVZ	NVZ	SVZ	EVZ	EVZ	EVZ	EVZ
Volcanic system	Reykjanes	Hengill	Bárðarbunga	Ljósufjöll	Eyjafjallajökull	Eyjafjallajökull	Eyjafjallajökull	Vestmannaeyjar
Fo	89.3–91.0	71.8–86.0	85.7–88.7	83.2–90.1	83.0–89.8	80.7–89.2	78.7–86.9	85.07–89.03
$^{3}He/^{4}He$	10.29–11.49	–	15.33–16.79	8.54	17.13	–	–	13.11–14.51
$^{206}Pb/^{204}Pb$	18.297	–	18.343–18.361	19.1335	19.2155	–	–	19.0467
$^{207}Pb/^{204}Pb$	15.48	–	15.420–15.427	15.5388	15.5566	–	–	15.5419
$^{208}Pb/^{204}Pb$	38.061	–	37.935–37.964	38.7567	38.8690	–	–	38.6541
$^{87}Sr/^{86}Sr$	0.703039	–	0.703036–0.703079	0.703400	0.703335	–	0.703241–0.703259	0.703138–0.703196
$^{143}Nd/^{144}Nd$	0.51313	–	0.513058–0.513099	0.512934	0.512987	–	0.512985–0.513004	0.513015–0.513019
$\delta^{18}O_{olivine}$	4.68–5.03	–	4.43–4.74	5.00	4.74	–	5.43–5.96	5.01
$^{176}Hf/^{177}Hf$	–	–	–	0.283113	0.283093	–	–	0.283103–0.283152
Age	10–13 ka	< 730 ka	< 730 ka	4000 a	587 ± 31 ka	< 730 ka	2010 AD	~ 5000–6000 ka

See Supplementary Material for data sources affiliated to respective cells

[a]Rock types according to Jakobsson et al. (2008). All samples are in fact subalkaline in composition

[b]Eyjafjallajökull 2010 summit eruption tephra is a mixture of benmoreite and basalt

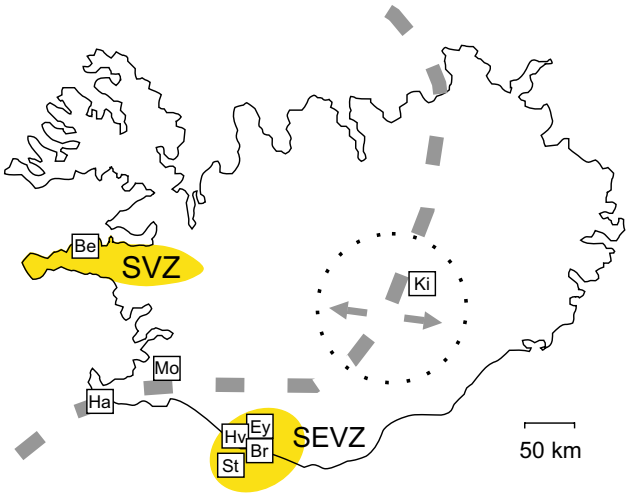

Fig. 1 Map of Iceland with sample locations: *Be* Berserkjahraun, *Ha* Háleyjabunga, *Mo* Mosfellsheiði, *Ki* Kistufell, *Hv* Hvammsmúli, *Ey* Eyjafjallajökull 2010, *Br* Brattaskjól, and *St* Stórhöfði. Approximate location of the plate boundary and the locus of the Iceland mantle plume (Wolfe et al. 1997) are marked with grey and black stippled lines, respectively. The major off-rift volcanic zones, Snæfellsnes Volcanic Zone (SVZ) and the southern tip of Eastern Volcanic Zone (SEVZ), are marked in yellow

Reykjavík with $Fo_{71.8–86.0}$ olivines. Kistufell is a monogenetic table mountain located at the NW margin of the Vatnajökull ice cap (Breddam 2002), close to the inferred center of the Iceland plume at the rift axis (Wolfe et al. 1997). The Kistufell magma has been interpreted as plume-derived near-primary melt, and it has up to $Fo_{88.7}$ olivines (Breddam 2002). The exact age of Kistufell is unknown, but is probably close to the end of the last glacial period (Breddam 2002).

Olivines from off-rift volcanic zones

The sampled lavas and tephra from SVZ and SEVZ (Berserkjahraun, Hvammsmúli, Brattaskjól and Stórhöfði lavas, and Eyjafjallajökull 2010 tephra) were erupted from off-rift volcanic systems situated in areas of minimal crustal extension (Fig. 1). Off-rift volcanoes are peripheral to the main rift zone and they produce alkaline or mildly alkaline lavas enriched in incompatible elements compared to rift tholeiites (Jakobsson 1972; Hemond et al. 1993). This indicates relatively small degree of mantle melting (Sæmundsson 1979), while isotopic composition (especially high $^{206}Pb/^{204}Pb$) suggests a more enriched mantle source (Kokfelt et al. 2006; Peate et al. 2010). This covariation of small degree mantle melting and enriched isotopic composition is commonly explained by a model where smaller degree melting allows preferential tapping of enriched and fusible veins set in a more refractory mantle (Chauvel and Hémond 2000; Fitton et al. 2003; Kokfelt et al. 2006).

The tectonic setting of the two major off-rift volcanic zones, SVZ and SEVZ (Fig. 1), is different. SVZ has been interpreted as a zone of weakness that is the remnant of the Snæfellsnes-Skagi paleo-rift (Hardarson et al. 1997), active from 15–20 to 10–12 Ma (Martin et al. 2011). In contrast, magmatism in South Iceland is related to the southward propagation of the Eastern Volcanic Zone (EVZ), which is the youngest (activated > 3 Ma, Martin et al. 2011) volcanically active zone in Iceland, and the most profuse magma producer in historical times (Thordarson and Larsen 2007). In this area, including the Eyjafjallajökull and Vestmannaeyjar volcanic systems, active extension is minimal. Of SEVZ and SVZ lavas, the latter have higher La/Yb_N (2–12 vs 2–7), indicating smaller degrees of melting, as well as lower ε_{Nd}, and lower $^3He/^4He$ (Peate et al. 2010).

Three locations from SVZ were analyzed for olivine trace elements compositions by Sobolev et al. (2007): Enni, Sydri-Raudamelur and Ydri-Raudamelur. Due to these SVZ olivine data already existing, we sampled only one SVZ lava, Berserkjahraun (Fig. 1, Table 1). Berserkjahraun is one of the most primitive of SVZ lavas (Peate et al. 2010), erupted within the Ljósufjöll volcanic system, and inferred to be younger than 4000 a in age (Jóhannesson 1994). Our sample of Berserkjahraun lava has $Fo_{83.2–90.1}$ olivines.

Our SEVZ sample set includes olivine macrocrysts from three samples from Eyjafjallajökull volcanic system and one sample from Vestmannaeyjar volcanic system (Fig. 1, Table 1). Brattaskjól and Hvammsmúli samples are from macrocryst-rich transitional basalts (often referred to as ankaramites) from the southern slope of the volcano. Hvammsmúli is 600 ka in age (Wiese 1992), a 45 m thick outcrop that has been interpreted as a remnant of a lava lake (Loughlin 1995), whereas Brattaskjól is a less studied macrocryst-rich basalt 4 km east of Hvammsmúli. Our Hvammsmúli and Brattaskjól samples have up to $Fo_{89.8}$ and $Fo_{89.2}$ olivines, respectively.

Our "Eyjafjallajökull 2010" sample comprises forsteritic olivines from tephra of the Eyjafjallajökull 2010 eruption. This eruption was a mixed eruption of benmoreite and basalt, which carried olivine with diverse compositions ($Fo_{74–87}$). The 2010 summit eruption followed an effusive flank eruption on the Fimmvörðuháls pass, and it was the intrusion of Fimmvörðuháls parental magma into a silicic magma chamber that ignited the summit eruption (Sigmarsson et al. 2011). The olivine crystals of Fimmvörðuháls have been extensively studied (Sigmarsson et al. 2011; Viccaro et al. 2016; Pankhurst et al. 2018), and due to the co-genetic nature of Fimmvörðuháls basalt and Eyjafjallajökull 2010 tephra, they likely carry similar olivine macrocrysts.

Our olivine samples from Vestmannaeyjar were collected from the Stórhöfði lava flow field at the southern tip of Heimaey Island. According to Jakobsson (1968, 1979), Stórhöfði lava erupted during the Holocene and is slightly

older than 5470 ± 160 years in age (Mattsson and Höskuldsson 2003). It is the most primitive lava flow field on Heimaey, compositionally similar to the Surtsey 1963–1967 eruption (Mattsson and Oskarsson 2005), and it has up to Fo_{89} olivines. The Stórhöfði sample examined in this study is from a tube-fed lava flow related to a late phase of the eruption (Mattsson and Oskarsson 2005).

Methods

Electron probe microanalysis

The microprobe analyses of major and trace element compositions of olivine crystals were conducted at the Institute of Earth Sciences, University of Iceland using the JEOL JXA-8230 electron microprobe. Olivine macrocrysts were hand-picked from crushed and sieved (Ø = 0.1–4.0 mm) rock samples and mounted in 1-inch epoxy molds or glass slides, except for the Mosfellsheiði sample, for which olivines were analyzed directly from 1-inch glass slides made of polished rock. Polished sample surfaces were cleaned with ethanol and carbon coated before the electron probe and laser ablation analyses. For the high-precision trace element analyses of olivine cores, we utilized a modified version of the high-probe current protocol by Batanova et al. (2015) with an acceleration voltage of 20 kV and 500 nA beam current. These analyses were focused on forsteritic olivines using low brightness of BSE images as an indicator of high Mg content, and the analyses targeted the geometric, compositionally homogenous, center of the olivine crystals. The resulting instrumental precisions for Ni and Mn are 0.52% and 0.48% relative standard deviations, respectively. When measuring traverses across olivine zonation, we used shorter analysis time, 15 kV accelerating voltage and 20 nA probe current. This setup delivers precise Fo measurements (~0.5% standard error) but relatively low precision on trace elements, e.g. an average 6.5% standard error for Ni. Detailed information of analytical conditions and standards are given in Supplementary Material.

LA–ICP–MS analysis

LA–ICP–MS analyses were carried out at the Department of Geosciences and Geography, University of Helsinki using a Coherent GeoLas Pro MV 193 nm laser ablation system connected to an Agilent 7900 s quadrupole ICP–MS equipped with high-sensitivity ion lens configuration and Pt interface cones. The following isotopes were included in the measurement program: ^{7}Li, ^{23}Na, ^{24}Mg, ^{25}Mg, ^{27}Al, ^{29}Si, ^{43}Ca, ^{31}P, ^{43}Ca, ^{44}Ca, ^{45}Sc, ^{49}Ti, ^{51}V, ^{52}Cr, ^{55}Mn, ^{56}Fe, ^{57}Fe, ^{59}Co, ^{60}Ni, ^{62}Ni, ^{63}Cu, ^{66}Zn, ^{85}Rb, ^{88}Sr, ^{137}Ba. The olivine macrocrysts were ablated up to three times at the center of the crystals with a spot size of 44 µm and laser energy densities of 7 J/cm^2. Sample measurements were bracketed by analyses of reference materials NIST SRM 610 (Spandler et al. 2011) and GSE 1G (Jochum et al. 2005) at fluences of 10 J/cm^2. External standardization using GSE 1G synthetic basalt glass yielded better reproduction of EPMA compositional data than NIST SRM 610, and therefore, all data reported here were externally standardized against GSE 1G. Data reduction was carried out using the SILLS software package (Guillong et al. 2008). To avoid problems arising from Fe–Mg zoning in some olivine grains and the different sampling spot sizes of LA–ICP–MS and EPMA, internal standardization was done using Si concentrations as determined by EPMA. Further information on the analytical procedure and complete summary of instrumental parameters is given in the Supplementary Material.

Results

Compositional zonation in olivine

Olivine crystals in the analyzed samples vary in size (0.3–3.4 mm in diameter) and compositional zoning (Fig. 2). The largest crystals analyzed are from Hvammsmúli (0.5–3.4 mm), followed by Mosfellsheiði (0.5–2.5 mm), Brattaskjól (0.5–2.4 mm), Kistufell (0.3–2.3 mm), Háleyjabunga (0.5–2.2 mm), Berserkjahraun (0.6–2.2 mm), Eyjafjallajökull 2010 (0.5–2.0 mm), and Stórhöfði (0.4–1.3 mm). Mg–Fe compositional zoning rims are very thin (< 20 µm), or absent, in olivines from Háleyjabunga (Fig. 2a) and Kistufell. $Fo_{>86}$ olivine crystals from Brattaskjól have thin (up to 120 µm) normally zoned rims (i.e. Fe increases towards the edge; Fig. 2b), whereas reverse zoning (i.e. Mg increases towards the edge) is present in $Fo_{<86}$ olivines. Mg–Fe zoned rims in analyzed olivines from the Eyjafjallajökull 2010 sample are dominantly less than 100 µm in thickness and normally zoned. Moderately thick, 100–200 µm normally zoned rims characterizes the Stórhöfði and Berserkjahraun olivines. Mosfellsheiði and Hvammsmúli olivine macrocrysts have the broadest Mg–Fe zoned rims, up to 220 µm and 700 µm (Fig. 2c) in thickness, respectively.

We analyzed the zoning patterns along rim-to-core traverses in olivines from Hvammsmúli, Brattaskjól and Mosfellsheiði. Nearly all of the analyses of Hvammsmúli (19/19), Brattaskjól (10/12) and Mosfellsheiði (3/3) revealed decoupling of Fo and Ni in the Mg–Fe zoned parts of the crystals (Fig. 3), a phenomenon earlier reported by Lynn et al. (2017) from Hawaiian olivines. In Hvammsmúli olivine 'Pos–1a_Ol1', the Ni content becomes constant 190 µm from the crystal edge, whereas Mg–Fe zonation extends 520 µm from the crystal edge to core (Fig. 3).

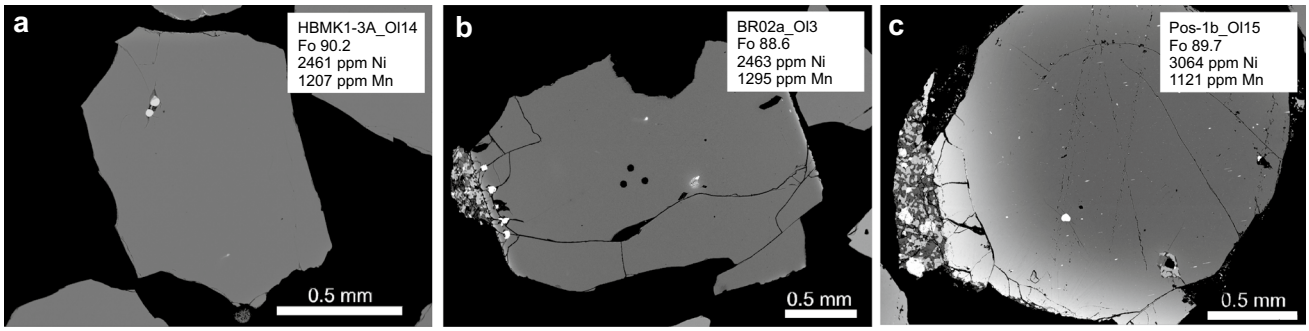

Fig. 2 Three olivine macrocrysts mounted in epoxy resin and selected to display difference in breadth of Mg–Fe compositional zoning between sampling locations **a** Háleyjabunga olivine (no.14) with thinner than 20 µm Mg–Fe zoning. **b** Brattaskjól olivine (no. 3) with a 90 µm thick Mg–Fe zoned rim. The three dots at the center are laser ablation pits. **c** Hvammsmúli olivine (no. 15) with a thick, 700 µm broad, Mg–Fe zoned rim

The broadest Mg–Fe zoning analyzed from Hvammsmúli olivines is 700 µm thick from rim to core (olivine Pos-1b_Ol15, Fig. 2c), while Ni zoning only extends ~500 µm from the rim (Fig. 2c). Zoning patterns in normally zoned Mosfellsheiði and Brattaskjól olivines are variable and thinner. Ni zonation extends 30–180 µm and 20–100 µm from the crystal edge towards the crystal cores for Mosfellsheiði and Brattaskjól olivines, respectively, while the width of the Mg–Fe zoned rims varies in the range 120–220 µm in Mosfellsheiði and 50–100 µm in Brattaskjól.

Major and trace elements in olivine

Major and trace element composition in the olivine macrocrysts examined is illustrated in Figs. 4 and 5, and the full dataset is included in the Supplementary Material. Olivine data from Kistufell and Háleyjabunga are found consistent with earlier analyses acquired by Sobolev et al. (2007) and Neave et al. (2018) (see Supplementary Material). The lowest Ni and highest Mn relative to Fo content were measured in olivines from Háleyjabunga and Berserkjahraun. Olivines from these two sampling locations define continuous linear trends on Mn vs. Fo and Ni vs. Fo plots (Fig. 4) and, at Fo_{90}, both have ~2500 ppm Ni and ~1200 ppm Mn. Kistufell and Mosfellsheiði olivine macrocrysts have higher Ni and lower Mn, and define a single trend in the Mn-Fo space (Fig. 4a). Kistufell has primitive $Fo_{88.15}$ olivines, whereas Mosfellsheiði olivines are relatively evolved ($Fo_{<86}$).

Compared to olivines from the rift-zones and SVZ, the SEVZ olivine macrocrysts have higher Ni and lower Mn contents at a given Fo content (Fig. 4). Values of Fo, Ni, Mn and Ca are similar in olivines from Hvammsmúli and Brattaskjól, although Hvammsmúli olivine are somewhat more forsteritic and have the highest Ni and lowest Mn (3536 ppm Ni and 1086 ppm Mn as compared to 3105 ppm Ni and 1189 ppm Mn in Brattaskjól). These two localities are combined for clarity as "Eyjafjallajökull lavas" in Fig. 4

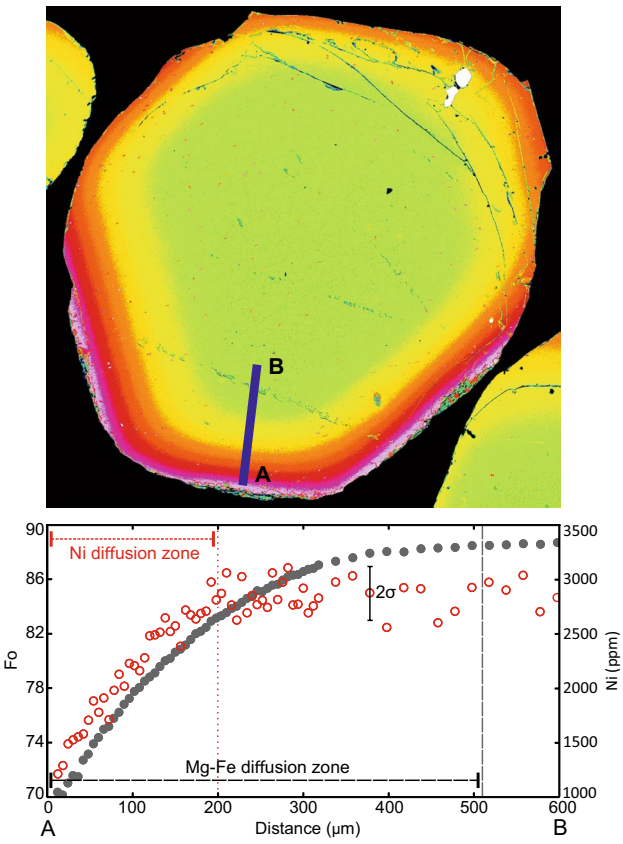

Fig. 3 Traverse across the zoning of Hvammsmúli olivine macrocryst (Pos-1a_Ol1). Location of the traverse shown on the upper false color olivine image, where yellow–green shades represent $Fo_{>80}$ olivine, and red–purple shades more ferrous ($Fo_{<80}$) compositions. In the lower graph, Fo and Ni variation at the edge segment (**a** through **b**) is shown. Near crystal edges, depressed Fo content ("Mg–Fe diffusion zone") extends farther towards the crystal core than lowered Ni ("Ni diffusion zone"). Average 2σ analytical error for Ni analyses is shown, while the propagated standard error in Fo content is approximately the size of the symbol

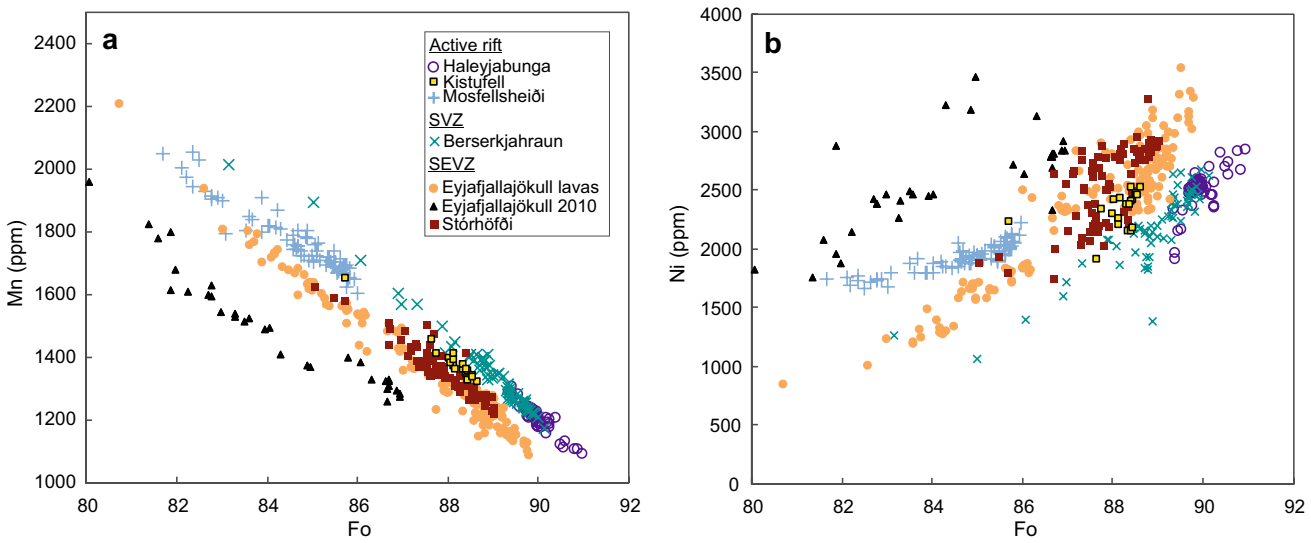

Fig. 4 **a** Mn and **b** Ni contents as a function of Fo content in olivine. Analytical error is equal or smaller than the symbol size

(compare to Fig. 8). In these lavas, there is a large trace element variability in the high-Fo primitive olivines compared to the more evolved. $Fo_{88.3–89.5}$ olivines have 1σ variations of ± 242 ppm for Ni, ± 50 ppm for Mn and ± 272 ppm for Ca in comparison to, e.g., $Fo_{85.0–86.2}$ olivines with 1σ of ± 89 ppm for Ni, ± 33 ppm for Mn and ± 93 ppm for Ca. Olivines with the lowest Ni and highest Mn in the $Fo_{88.3–89.5}$ population resemble Kistufell olivines (2350 ppm Ni and 1340 ppm Mn in Kistufell; Fig. 4), whereas the high-Ni olivines have 3360 ppm Ni and 1130 ppm Mn in average. Similarly, primitive olivines from Stórhöfði exhibit relatively large variability in trace element contents, and Eyjafjallajökull lavas and Stórhöfði form a unified linear array in the Mn vs. Fo diagram (Fig. 4). Olivine macrocrysts from the Eyjafjallajökull 2010 summit eruption have distinctively low Mn (Fig. 4a) and high Ni (Fig. 4b) in relation to the Fo content. The highest Ni is 3455 ppm in Fo_{85} olivine, whereas the more primitive olivines nearing Fo_{87} have more modest 2800–2920 ppm Ni. In addition, Ca contents in the Eyjafjallajökull 2010 olivines are low (1523 ppm on average).

Selected olivine macrocrysts from Hvammsmúli, Brattaskjól, Kistufell and Háleyjabunga were also analyzed with LA–ICP–MS for concentrations of Li, Na, Al, P, Ca, Sc, Ti, V, Cr, Mn, Co, Ni, Cu and Zn. At a given Fo, SEVZ olivines (Hvammsmúli and Brattaskjól) have lower Sc, and higher Li, Ti, Cr, Cu, and Zn, than Háleyjabunga (Fig. 5). The separate trends of SEVZ and Háleyjabunga olivines are outside of the analytical uncertainty; however, the compositions of Kistufell olivine macrocrysts overlaps the complete compositional variability detected in many trace elements (Sc, Ti, V and Al; Fig. 5). There is no significant difference in Co content, at a given Fo, between the locations. Brattaskjól olivine macrocrysts stand out with elevated Cr and Na in relation to the other samples. Our analyses of Háleyjabunga olivines are in agreement with earlier measurements by Neave et al. (2018), although our analyses have marginally higher Co contents. In turn, our SEVZ olivines resemble Neave et al. (2018) Stapafell olivines, with the exception that SEVZ olivines have higher Ti, Zn and Cu contents (Fig. 5).

Discussion

Ni, Mn and Ca in Iceland olivine macrocryst record

The major and trace element composition of Háleyjabunga and Berserkjahraun olivine macrocrysts resembles MORB olivines with low Ni and high Mn contents, and are compatible with the Herzberg (2011) model of olivine crystallizing from peridotite-derived melts and their derivate melts along Liquid Line of Descent (LLD, Fig. 6) at low pressure. Kistufell and Mosfellsheiði olivines, although richer in Ni and lower in Mn, are also consistent with peridotite melting, as long as melt mixing is allowed (red mixing lines in Fig. 6b). Mixing of primary and fractionated magmas can slightly elevate Ni in olivine relative to its Fo content (Herzberg et al. 2016). Ni contents in Mosfellsheiði olivines do not change over a range of Fo content (Fig. 6a), which may indicate cotectic crystallization of Ol + Plg + Cpx. Ca content in Háleyjabunga, Berserkjahraun, Kistufell and Mosfellsheiði olivine is compatible to Herzberg (2011) model of olivine crystallization from a peridotite source, except for a few Berserkjahraun olivines (Fig. 6c). In essence, the SVZ and rift-zone olivines in our dataset conform with lherzolite-sourced partial melts and the previous olivine data

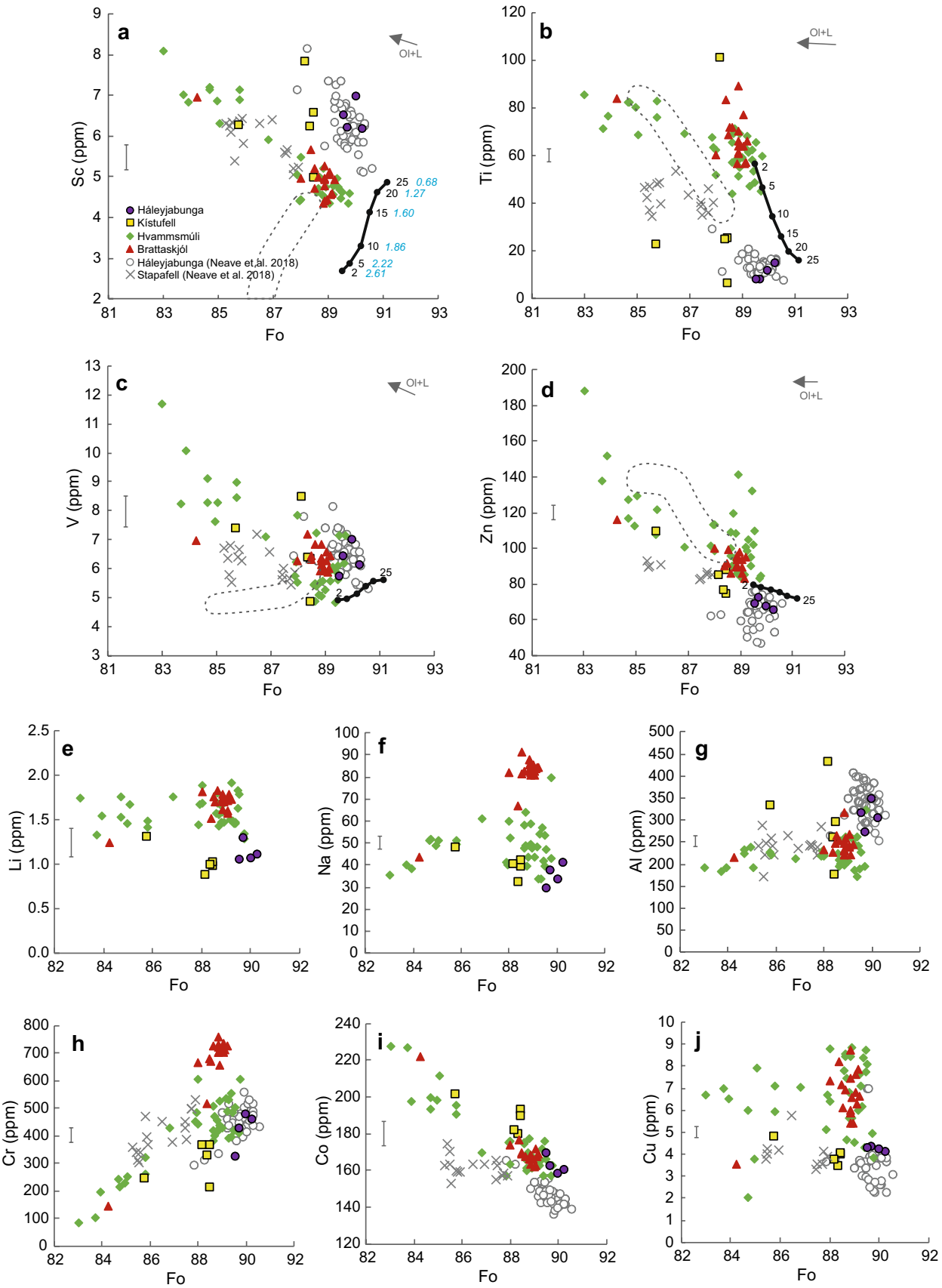
a
Sc (ppm)
Fo
Ol+L
Háleyjabunga
Kístufell
Hvammsmúli
Brattaskjól
Háleyjabunga (Neave et,ál. 2018)
Stapafell (Neave et al. 2018)
25 0.68
20 1.27
15 1.60
10 1.86
5 2.22
2 2.61
b
Ti (ppm)
c
V (ppm)
d
Zn (ppm)
e
Li (ppm)
f
Na (ppm)
g
Al (ppm)
h
Cr (ppm)
i
Co (ppm)
j
Cu (ppm)

◂**Fig. 5** **a**–**j** Sc, Ti V, Zn, Li, Na, Al, Cr, Co and Cu contents of Háleyjabunga, Stapafell, Kistufell, Hvammsmúli and Brattaskjól olivines. Compositions of model olivines crystallizing from accumulated near-fractional melts of KLB-1 mantle lherzolite (Hirose and Kushiro 1993) are indicated by the black line (cf. Sect. 5.5 for model details). Stippled field outlines the model olivine compositions in equilibrium with F5–40% melts of modally enriched KG2 peridotite (Kogiso et al. 1998). Labels in black and blue correspond to the degree of partial melting in percent (F%) and melt derivation pressures in GPa, respectively. Grey arrow marks the compositional vector produced by fractional crystallization of olivine; however, assumption of olivine-only crystallization has been shown true only for Háleyjabunga (Neave et al. 2018). Average instrumental 2σ errors are indicated by grey bars for the trace elements, whereas errors in Fo are smaller than the symbols used. Olivine Fo content is taken from EPMA analyses, whereas all trace element data is from LA-ICP-MS analyses. Háleyjabunga and Stapafell olivine compositions from Neave et al. (2018) are included for comparison

(Shorttle and Maclennan 2011; Herzberg et al. 2016; Neave et al. 2018).

Some olivines from Eyjafjallajökull and Vestmannaeyjar volcanic systems at SEVZ, however, have higher Ni contents and Fe/Mn ratios than previously published from Iceland (Fig. 6a, b). High Fe/Mn and Ni correlate in the high-Fo SEVZ olivine macrocrysts, and some of the high-Ni and high-Fe/Mn olivines, especially from the Eyjafjallajökull 2010 tephra, have low Ca (Fig. 6c). Many of the SEVZ olivines are outside the compositional range expected to crystallize from peridotite-derived melts as defined by Herzberg (2011) and may imply melting of an olivine-free mantle source (Sobolev et al. 2005) or relatively deep mantle melting combined with shallow olivine crystallization (Matzen et al. 2013, 2017a, b).

Trace elements concentrations in olivine couple strongly with Fo content. Thus, meaningful comparison of olivine compositions from different localities is achieved by normalizing the trace element contents by FeO or MgO, and by limiting the comparison to high-Fo olivines. In Fig. 7, we compare high-precision $Fo_{>86}$ olivine compositional data from SEVZ and other localities in Iceland (Sobolev et al. 2007, and this study) by utilizing Kernel density estimation (Green et al. 1988) of the probability density distribution of olivine compositions. Although SEVZ olivine compositions overlap with olivine from elsewhere in Iceland (Rift-zones and SVZ), Fig. 7 exhibits clearly how SEVZ has higher Ni and lower Mn in relation to olivine Fo. The Iceland rift-zone and SVZ olivine Ni data is somewhat bimodal, with two Ni(Mg/Fe)/100 probability density peaks at ~ 0.6 and ~ 0.7. This is not an artefact of combining our and Sobolev et al. (2007) datasets, but the result of elevated Ni in some Icelandic olivine. Herzberg et al. (2016) explained the elevated Ni in some Iceland olivine by mixing of near-primary and evolved melts derived from the same initially low-Ni, high-Mn peridotite sourced partial melt (see fig. 7 in Herzberg et al. 2016). The bimodality in SEVZ data (Fig. 7b) is solely produced by the Eyjafjallajökull 2010 olivines that have high Fe/Mn.

Indications of melt mixing

The SEVZ high-Fo olivines exhibit large variability in Ni, Mn and Ca contents, which decreases with decreasing Fo (Fig. 6). This is most evident in Brattaskjól and Hvammsmúli olivines, with $Fo_{<88.2}$ grains conforming to a crystal line of descent at low pressure and $Fo_{88.3–89.5}$ olivines exhibiting high variability in trace element contents (Fig. 8). In this high-Fo olivine population, there is an inverse correlation in Ni and Mn ($R^2 = 0.498$), and Ni and Ca ($R^2 = 0.486$). We interpret this compositional characteristic by mixing of near-primary mantle melts with initially varying Ni, Mn, and Ca.

The Hvammsmúli and Brattaskjól $Fo_{>88.2}$ olivines may initially have had variable Fo contents, which may have been later suppressed by diffusive re-equilibration with a carrier melt during crustal storage (Costa and Morgan 2010). During this process, variation in some trace elements (e.g. Ca) could have been retained due to their slower diffusion compared to Mg–Fe (e.g. Dohmen et al. 2007). Therefore, in theory, the high variability in trace element compositions in similar Fo olivines in Hvammsmúli and Brattaskjól could be a consequence of this incomplete re-equilibration process. This model is, however, hampered by the similar diffusion rates of Mn and Mg–Fe (Dohmen et al. 2007). Mn concentrations should have been similarly suppressed during diffusive re-equilibration as Fo contents, and we do not see this in the data (Fig. 8). In addition, the detected variation in Ca in olivines is so large (~ 1100 ppm, Figs. 6 and 8b), that producing it by olivine fractionation is improbable. Due to this reasoning, we favor mixing of two melts with significantly different Ca, Mn and Ni contents as the explanation for the high variability in the SEVZ olivine trace element contents. For Brattaskjól and Hvammsmúli, the higher Fo mixing end member has high Ni and relatively low Mn and Ca, whereas the more evolved member has lower Ni and higher Mn and Ca (Fig. 8).

High compositional variability is typical for high-Fo olivine-hosted melt inclusions of Icelandic magmas (Maclennan 2008a, b; Neave et al. 2013). This variability in the melt inclusion record (e.g. highly varying La/Yb) decreases as olivines become more evolved (ferrous), and the average composition of the olivine-hosted melt inclusions approaches the composition of the host magma. Maclennan (2008a) concluded that this phenomenon is consequential to mixing and homogenization of diverse mantle melts in the mid–lower crust. The major and trace element trends in Brattaskjól and Hvammsmúli olivine populations may indicate the same phenomenon: mixing of mantle melts derived from different depths and different

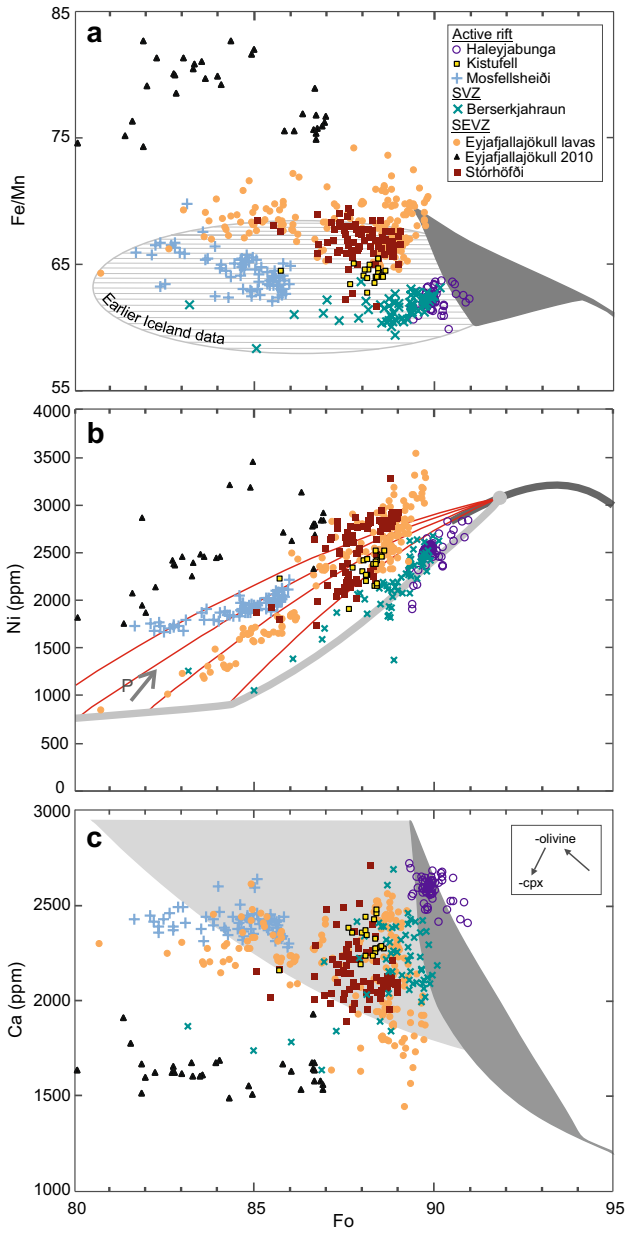

Fig. 6 Fe/Mn, Ni and Ca variation against Fo content of olivine crystals. Model olivine compositions adopted from Herzberg (2011) and Herzberg et al. (2016). "Eyjafjallajökull lavas" refer to the adjacent Hvammsmúli and Brattaskjól sampling locations. Higher Fe/Mn, Ni, and larger compositional variability at a given Fo content are evident for SEVZ magmas. **a** Olivine compositions in equilibrium with partial melts of peridotite source with 0.13% MnO marked with a gray field. Lined area defines the range of previous Iceland olivine data from Sobolev et al. (2007) and Neave et al. (2018). Olivine dominated fractional crystallization or mixing of basaltic magmas does not substantially change Fe/Mn in olivines. **b** The dark grey curve defines model olivine crystallizing from partial melts of peridotite (1964 ppm Ni) and the light grey curve describes olivine crystallizing along Liquid Line of Descent (LLD, primitive melt with 17.6% MgO). The LLD is calculated for 1 atm pressure; increase in pressure would hasten the onset of Cpx crystallization (arrow labelled 'P'). Red curves are olivine compositions that would crystallize from magmas that are mixtures of primary magma and derivate magmas along the LLD. **c** Dark grey field is model olivine of a peridotite source primary magma with 3.45 wt% CaO and 8–38 wt% MgO. The light grey area resembles model olivine crystallizing from derivate magmas with 8–20 wt% MgO. Analytical error is smaller than the symbol size

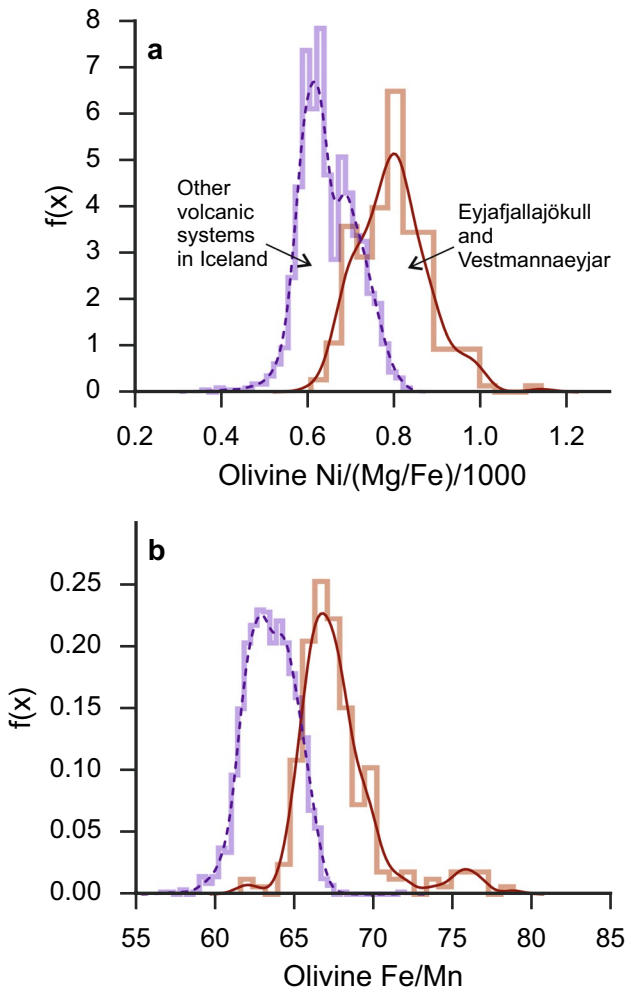

Fig. 7 $Fo_{>86}$ olivine trace element compositions from Sobolev et al. (2007) and this paper plotted as probability density against **a** olivine Ni/(Fe/Mg)/1000, **b** Olivine Fe/Mn. Dark lines are the Kernel Density Estimates of the data, and paler shades show the underlying histograms. SEVZ olivine data illustrated with red solid line and all other Iceland olivine compositions in violet stippled line. Higher values can be seen to represent higher contribution of pyroxenite mantle (e.g. Sobolev et al. 2007) or higher temperature difference between mantle melting and olivine crystallization (Matzen et al. 2013, 2017a, b)

rock-types from the mantle melting column. Furthermore, the variability in Brattaskjól and Hvammsmúli olivine trace element compositions indicates that the $Fo_{88.2–89.6}$ olivine population has had sufficiently short residence time in the magmatic environment not to be completely homogenized by diffusive re-equilibration.

High-P fractionation of clinopyroxene

Early fractionation of clinopyroxene has been proposed to explain elevated Ni and Fe/Mn and low Ca in olivines in some of the lavas of the North Atlantic Igneous Province

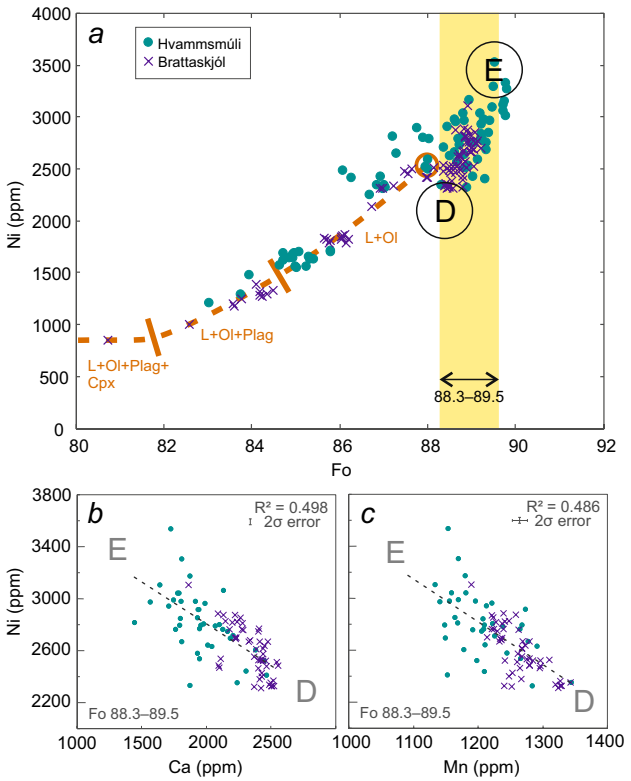

Fig. 8 **a** The observed steep Fo vs Ni trend of the Eyjafjallajökull transitional basalts (Hvammsmúli and Brattaskjól), interpreted as a mixing trend of two different mantle melts, one with high Ni (denoted with 'E' for enriched in Ni) and other with low Ni ('D' for depleted in Ni). The orange stippled line defines model olivine compositions that crystallize along Liquid Line of Descent (LLD) from a melt with equilibrium olivine composition 2500 ppm Ni at Fo_{88} (orange circle). These model olivine compositions have been calculated using the Beattie et al. (1991) model of olivine-liquid Ni partitioning and Þeistareykir initial melt composition (the same as used for the model olivines crystallizing along LLD in Fig. 6) with added 200 ppm Ni. The Þeistareykir initial melt composition was calculated with PRIMELT3 MEGA.xlsm (Herzberg and Asimow 2015). The yellow field marks the Fo range of the mixing trend and the olivine shown in the subplots **b** and **c**. In subplot **b** Ni vs Ca and **c** Ni vs Mn in $Fo_{88.3–89.5}$ olivine

(Hole 2018). Also, particular geochemical trends in Vestmannaeyjar lavas in SEVZ, specifically decreasing CaO/Al_2O_3 and Sc/Y with lowering MgO, have been explained by high-P (0.6–1.0 GPa) clinopyroxene crystallization (Furman et al. 1991; Mattsson and Oskarsson 2005). Against this backdrop, and considering that we assume olivine-dominated fractional crystallization for the Iceland magmas (Fig. 6), it is important to evaluate whether high-P clinopyroxene crystallization may have influenced the SEVZ olivine record.

The stability field of clinopyroxene expands at the expense of olivine at high P and clinopyroxene becomes a liquidus phase in progressively more primitive melts (O'Hara 1968); clinopyroxene crystallization can thus commence in near-primary mantle melts at high pressures. Crystallization of Ca-rich clinopyroxene lowers Ca and elevates Fe/Mn in the melt, and olivine crystallizing along with clinopyroxene may, therefore, be imprinted by higher Fe/Mn (Herzberg et al. 2013) and lower Ca (Hole 2018) than olivine crystallizing in the absence of clinopyroxene. Furthermore, Ni is not as compatible in clinopyroxene as in olivine, and therefore, the Ni content of mafic magmas can stay relatively elevated if clinopyroxene crystallization is initiated early in the crystallization sequence (Hole 2018).

It is unlikely that high-P fractionation of clinopyroxene could have produced the high Ni and low Mn contents in $Fo_{>88}$ olivines in Brattaskjól, Hvammsmúli and Stórhöfði, as clinopyroxene fractionation does not enrich melts in Ni, and thus cannot elevate Ni in olivines above the initial mantle-derived values. In addition, the trends of Ni and Ca against Fo content in olivines are not suggestive of clinopyroxene fractionation (i.e. steep depletion in Ni and enrichment in Ca in lower-Fo olivine, Fig. 6) for these localities. Olivine macrocrysts from the Eyjafjallajökull 2010 eruption tephra, however, may have been affected, as they are relatively evolved ($Fo_{<86.9}$), very poor in Ca and Mn, and show an increase in Fe/Mn (Fig. 6a) at $Fo_{82–85}$. Moreover, the relatively flat Ni versus Fo trend is suggestive of cotectic crystallization of olivine + clinopyroxene + plagioclase (Fig. 6b). These trace element characteristics comply with fractionation of clinopyroxene and olivine at high pressures, and thus the highest Fe/Mn values acquired from Eyjafjallajökull 2010 olivines (Figs. 6a and 7b) may have been affected by the early initiation of clinopyroxene crystallization.

Ni/Fo-decoupling in zoned olivine macrocrysts

Decoupled Fe–Mg and Ni in olivine rims likely reflects faster diffusion of Fe–Mg than Ni during re-equilibration of olivine and carrier melt (Lynn et al. 2017; Neave et al. 2018). We observed this decoupling in nearly all Hvammsmúli, Mosfellsheiði and Brattaskjól olivines. Considering the maximum thickness of olivine zonation in these localities, this phenomenon may have affected Ni/Fo ratio (by lowering Fo in relation to constant Ni) in crystal cores of Hvammsmúli olivines smaller than 1.4 mm, and Mosfellsheiði and Brattaskjól olivines smaller than 0.5 mm and 0.25 mm in diameter, respectively. Luckily, these locations host large olivine macrocrysts; therefore, only a few (potentially 13 out of 79) olivine core analyses of Hvammsmúli and none of the olivine core analyses of Mosfellsheiði or Brattaskjól may have been affected. In general, the Iceland olivine macrocryst record is dominated by large homogenous cores with thin zones of diffusive re-equilibration at crystal rims (e.g.

Thomson and Maclennan 2013). Hence, accidental analyses of Fe–Mg zoned olivine rims (with non-equilibrium Ni/Fo ratio) are improbable and unlikely to affect the current Iceland olivine trace element record (Shorttle and Maclennan 2011; Sobolev et al. 2007; Neave et al. 2018; and this study) to any significant degree.

Sc, Ti, V and Zn and their partitioning in mantle melting

In addition to the apparent enrichment in Ni coupled with lower Mn and Ca contents, SEVZ olivines have different Li, Sc, Ti, V, Zn and Cu contents in comparison to Háley-jabunga olivines (Fig. 5). This could be solely consequential to the greater depth and lower degree of mantle melting (F) at SEVZ, and it is uncertain, whether variation in the mantle source can be discerned based on these trace elements. To inspect this, we modelled partitioning of Sc, Ti, V and Zn during adiabatic near-fractional melting of KLB-1 lherzolite (Hirose and Kushiro 1993) at 1480 °C potential temperature (Matthews et al. 2016) and 0.5–4.0 GPa. In addition, we ran a similar melting model for the KG2 olivine-bearing pyroxenite–peridotite hybrid (Kogiso et al. 1998). Sc, Ti, V and Zn were chosen, because their partitioning has been determined at high-P conditions and sufficient partitioning coefficients were available (Davis et al. 2013; Laubier et al. 2014). Cu and Li were not modelled as their partitioning is yet poorly constrained, and since they are moderately incompatible to incompatible elements in mantle melting, their enrichment in SEVZ olivines (Fig. 5) likely reflects lower F, not variation in mantle mode (Ryan and Langmuir 1987; Lee et al. 2012). Al-depletion in SEVZ olivines in comparison to Háleyjabunga olivines, in turn, is likely consequential to higher Fo of Háleyjabunga olivines and the Mg-dependent partitioning of Al (Herzberg and O'Hara 2002).

The modelling of mantle melting was done with the pMELTS software (Ghiorso et al. 2002) with the ALPHAMELTS 1.8. front end (Smith and Asimow 2005). We used the correct version of pMELTS garnet model (Berman and Koziol 1991), and did not include Na_2O, K_2O, Cr_2O_3 and MnO into the initial mantle compositions. pMELTS has not been calibrated for MnO (Ghiorso et al. 2002), Cr_2O_3 was not included to avoid over-stabilization of spinel (Asimow et al. 1995), and Na_2O and K_2O were omitted to facilitate reliable estimation of the solidus (Lambart et al. 2012, 2016; Jennings et al. 2017). All models were done without imposed constrains on fO_2, although $fO_2 = FQM - 1$ was used to set Fe^{2+}/Fe^{3+} for the initial state. A 0.5 wt% threshold of melt extraction was used in all models, and a simple 1D melt aggregation column was assumed when assessing the composition of accumulated near-fractional partial melts at various pressures. After modelling mantle melting, we calculated the Fo and trace element content of olivine in equilibrium with the model mantle melts at 1 atm utilizing the parameterization of Herzberg and O'Hara (2002) and appropriate partitioning coefficients. The Supplementary Material provides the complete model conditions, initial mantle source compositions and partitioning coefficients.

Modally enriched mantle components, such as KG2, are thought to reside in the sub-Icelandic mantle as slivers in a more refractory matrix (Shorttle et al. 2014). Hence, our model melts of a one-component near-fractional mantle melting of KG2 do not fully suffice as an analogy for potential enriched Iceland melts. We opted for this simple setup, as developing a complex multi-component melting model for the sub-Icelandic mantle was not the aim of this study (cf. Shorttle and Maclennan 2011; Rudge et al. 2013; Shorttle et al. 2014; Lambart 2017 for existing parameterizations). The model olivine compositions of the KLB-1, and especially the KG2, partial melts are mainly illustrative and restricted by the limitations of pMELTS (cf. Rudge et al. 2013 and the Supplementary Material). Fo content in the KG2 model olivines should be treated with caution, as pMELTS performs poorly when calculating major element compositions in partial melts of modally enriched mantle lithologies (e.g. Lambart et al. 2016). The model olivine compositions are, however, useful for a qualitative estimation of whether typical KLB-1 lherzolite can explain the detected trace element variability in olivines, or whether lithological variation in the source is suggested.

The model olivine compositions crystallizing from KLB-1 and KG2 partial melts are shown in Fig. 5 and given in the Supplementary Material. The KLB-1 solidus is crossed at 3.2 GPa in the garnet stability field and garnet is in the residue until the spinel-garnet transition at 1.77 GPa. Spinel disappears from the residue at 1.63 GPa. The large stability range of garnet in comparison to spinel reflects limitations in the pMELTS garnet model and is partly due to omitting Cr_2O_3 from the calculations. Melt aggregation occurs over a large P-interval with a melt-fraction of 2% at 2.61 GPa, 5% at 2.22 GPa, 10% at 1.86 GPa, 15% at 1.60 GPa, 20% at 1.27 GPa and 25% at 0.68 GPa (Fig. 5a). According to the pMELTS model, the KG2 mantle is already 5% molten at 4 GPa, and this melt portion was handled as an isobaric batch melting at 4.00 GPa. Its melt fraction increases to 10% at 2.11 GPa, 15% at 1.78 GPa, 20% at 1.47 GPa, 25% at 1.30 GPa, 30% at 1.15 GPa, 40% at 0.99 GPa and 45% at 0.85 GPa. The accumulated partial melts are ferric, which manifests as low Fo content of the model olivines (Fig. 5).

The Sc, Ti, and V concentrations in the analyzed olivine crystals conform with model olivines crystallizing from partial melts of lherzolite mantle (KLB-1). Háleyjabunga olivines show compatibility with a high-degree melt of a spinel lherzolite, whereas Brattaskjól and Hvammsmúli

olivines seem to have crystallized from accumulated low-degree melts of mixed spinel and garnet lherzolite source (Fig. 5). Lower Sc in SEVZ olivines can be explained by greater depth of melting (Fig. 5a, higher D_{Sc} in garnet lherzolite compared to spinel lherzolite), whereas high Ti in SEVZ olivines is compatible with the lower F expected in off-rift setting (Fig. 5b). Differences in V can be also attributed to greater melting depth beneath SEVZ (Fig. 5c), but due to the strong dependency of V partitioning on fO_2 (Canil 1997; Laubier et al. 2014), the lower V in olivines may also reflect more oxidized nature of the SEVZ magmas. KG2-sourced model olivines have comparable Sc, Ti and V contents to those of KLB-1, although similar Sc and Ti values are reached at higher melt fractions (Fig. 5a–c).

Our KLB-1 lherzolite melting model does not explain the elevated Zn in SEVZ olivines, as Zn content is rather insusceptible to melting degree and melt derivation depth. In turn, KG2 model olivines have high Zn in comparison to KLB-1 melts (Fig. 5d), and thus the high Zn in SEVZ olivines may indicate the contribution of a modally (more pyroxene, less olivine) or compositionally (elevated Zn) enriched source in the mantle melting. Elevated Zn/Fe is a known property of many OIB magmas and has been proposed to indicate olivine-free pyroxenite in the mantle source (Le Roux et al. 2010, 2011). Alternatively, the lower Fo content in SEVZ olivines compared to Háleyjabunga, potentially implying a more differentiated host melt, may also contribute to the apparent Zn-enrichment in the SEVZ olivines. The olivine-liquid partitioning of Zn during fractional crystallization of basalts is yet inadequately constrained.

In essence, although Sc, Ti and V contents of the SEVZ olivines conform to olivine crystallizing from partial melts of KLB-1 lherzolite, the Zn enrichment may indicate that some enriched lithologies partake in melting in the mantle below. KG2-like peridotite–pyroxenite hybrid could be a good candidate for a potential enriched mantle lithology below Iceland, as it produces magmas with high-Fe/low-Ca (Shorttle et al. 2014) and, according to our analysis, does not significantly modify Sc, V, and Ti in olivines compared to 'normal lherzolite' values.

Origin of the SEVZ olivine signature

High Fe/Mn and Ni, and low Ca in olivine are attributes of olivine crystallized from a partial melt of olivine-free pyroxenite mantle (Sobolev et al. 2007). Following this rationale, the strongest affinity to 'pyroxenite source' is shown by the Eyjafjallajökull 2010 olivine macrocrysts, but also the other SEVZ samples show partial contribution of olivine-free source (Fig. 7). The highest-Ni Hvammsmúli, Brattaskjól and Stórhöfði olivines in SEVZ are comparable to, e.g., the ~ 70 Ma Quepos Terrane olivine from magmas of the Galapagos plume, for which olivine-free pyroxenite mantle source has been inferred (Trela et al. 2015). The parametrization of Gurenko et al. (2010):

$$X_{px} = 6.705 \times 10^{-4} \times \mathrm{Ni(ppm)} \times \frac{\mathrm{FeO}}{\mathrm{MgO}} - 1.332 \times 10^{-2} \times \frac{\mathrm{Mn(ppm)}}{\mathrm{FeO}} + 1.524, \quad (1)$$

implies 44–52 wt% and 64–77 wt% contribution of olivine-free pyroxenite-derived melt (X_{px}) to the parental melt of Hvammsmúli high-Ni (> 3000 ppm) and Eyjafjallajökull 2010 olivine macrocrysts, respectively.

Recent thermodynamic modelling suggests that the silicic melts of olivine-free pyroxenite are prone to react with the surrounding peridotite, and thus less likely to preserve their coherence and compositional signature and eventually crystallize olivine in the crust (Lambart 2017). In addition, as the concentrations of the transitional elements in the SEVZ olivines are compatible with a garnet lherzolite mantle source, large input from olivine-free source seems unlikely. Although some of the SEVZ olivines were found to be Zn-enriched, this does not necessarily argue for olivine-free source, as Zn-enrichment is also expected in partial melts of enriched olivine-bearing mantle types (e.g. KG2). Furthermore, the lower Ca in olivines does not indicate the absence of olivine in the mantle source either but may imply lower degree of mantle melting and source enrichment in clinopyroxene or garnet.

As large-scale contribution of magmas directly derived from olivine-free mantle (Px-1 or similar, Sobolev et al. 2007) seems unlikely for SEVZ magmatism, we proceed on deciphering the SEVZ olivines by means of relatively deep melting of olivine-bearing mantle. Also, even if the mantle signature in the SEVZ olivines was due to contribution of melts from olivine-free pyroxenite source, the mantle melting would occur deep anyhow, due to the lower solidus temperature and greater fusibility of olivine-free pyroxenite in comparison to common mantle peridotite (Lambart et al. 2016).

$D_{Ni}^{ol/liq}$ and $D_{Mn}^{ol/liq}$ are, directly (the former) and indirectly (the latter), temperature dependent (Matzen et al. 2013, 2017a, b), and elevated Ni and Mn in olivine can thus be related to the temperature difference between mantle melting and olivine crystallization ($-\Delta T_{m\text{-}c}$). The ratio between NiO in crystallizing equilibrium olivine ($NiO^{ol}@T_c$) and NiO content in olivine in the mantle ($NiO^{ol}@T_m$) relates to the temperature of olivine crystallization (T_c) and mantle melting (T_m) as follows (Matzen et al. 2017a):

$$\frac{NiO^{Ol}@T_c}{NiO^{Ol}@T_m} = \exp\frac{-\Delta_{r(1)}H^{\circ}_{T_{ref},P_{ref}}}{R}\left(\frac{1}{T_c} - \frac{1}{T_m}\right), \quad (2)$$

where $-\Delta_{r(1)}H^{\circ}_{T_{\mathrm{ref}},P_{\mathrm{ref}}}/R$ is the temperature dependency of $D^{\mathrm{ol/liq}}_{\mathrm{Ni}}$ (K), T_{c} and T_{m} are in Kelvin and $\mathrm{NiO}^{\mathrm{ol}}$ in weight units. This can be rearranged for the temperature difference between mantle equilibration and olivine crystallization ($\Delta T_{\mathrm{m-c}}$):

$$\Delta T_{\mathrm{m-c}} = \frac{-\ln \frac{\mathrm{NiO}^{\mathrm{Ol}}@T_{\mathrm{c}}}{\mathrm{NiO}^{\mathrm{Ol}}@T_{\mathrm{m}}}}{\left(-\Delta_{r(1)}H^{\circ}_{T_{\mathrm{ref}},P_{\mathrm{ref}}}/R\right)} + \frac{1}{T_{\mathrm{c}}}^{-1} - T_{\mathrm{c}}. \quad (3)$$

This equation allows estimation of the temperature at which the parental melt of the Ni-rich SEVZ olivine grains last equilibrated with the mantle. For the calculation, we used 0.43 wt% NiO for $\mathrm{NiO}^{\mathrm{ol}}@T_{\mathrm{c}}$, the same amount as in the five most Ni-rich SEVZ $\mathrm{Fo}_{>88.3}$ olivines, 2975 ppm Ni in mantle olivine ($\mathrm{NiO}^{\mathrm{ol}}@T_{\mathrm{m}}$), as in Herzberg et al. (2016), 4505 ± 196 K for the temperature dependency of Ni-partitioning ($-\Delta_{r(1)}H^{\circ}_{T_{\mathrm{ref}},P_{\mathrm{ref}}}/R$; Matzen et al. 2017a), and 1316 °C for near surface olivine crystallization temperature (T_{c}). The last is an average of published $\mathrm{Fo}_{>88.3}$ olivine crystallization temperatures from Holocene Icelandic lavas determined using olivine-spinel aluminum exchange thermometry (Matthews et al. 2016; Spice et al. 2016). It is to be noted that the selection of T_{c} has only minor effect on the calculated $\Delta T_{\mathrm{m-c}}$ within reasonable values (e.g. 1266–1447 °C), but the formalization is susceptible to uncertainty regarding Ni in mantle olivine (Matzen et al. 2017a).

With these parameters, Eq. 3 gives 75 ± 3 °C for the $-\Delta T_{\mathrm{m-c}}$, i.e. it indicates mantle-melt equilibration at 75 ± 3 °C higher T than the T of olivine crystallization. Using the slope of the olivine-saturated liquidus (55 °C/GPa, Sugawara 2000), $\Delta T_{\mathrm{m-c}}$ corresponds to 1.36 ± 0.06 GPa ΔP. If we assume olivine crystallization at surface (at 1 atm) and 3100 kg/m^3 average density for crust and refractory uppermost mantle, this pressure corresponds to ~45 km final mantle melting depth. This must be considered as the absolute minimum value for the inferred depth of melt equilibration in the mantle (final melting depth), as primitive olivine macrocrysts of Hvammsmúli and Stórhöfði likely crystallized at considerable pressure and depth, not at the surface. Crystallization pressures up to 0.6–1.0 GPa for Vestmannaeyjar and Eyjafjallajökull magmas have been proposed (Jakobsson et al. 1973; Furman et al. 1991; Sigmarsson 1996; Keiding and Sigmarsson 2012). If these pressures of olivine crystallization are considered and correspondingly elevated T_{c}'s are used (1349–1371 °C), final melting pressures of 2.0–2.5 GPa (i.e. depths of 66–81 km) are indicated. These pressures are close to the inferred pressure of spinel-garnet phase transition for KLB-1 lherzolite mantle (2.14–2.17 GPa, Jennings and Holland 2015).

Our estimation of final mantle-melt equilibration at > 45 km depth is considerably deeper than the crustal thickness at SEVZ (Darbyshire et al. 2000; Fedorova et al. 2005; Jenkins et al. 2018), but in line with the depth of the lithosphere–asthenosphere boundary (LAB) according to glacial isostatic adjustment studies (Árnadóttir et al. 2009; Barnhoorn et al. 2011). However, there is considerable uncertainty regarding the LAB in Iceland, with resent estimates of ridge centered lithospheric thicknesses varying in 10–60 km range (Pagli et al. 2007; Bjarnason and Schmeling 2009; Barnhoorn et al. 2011; Rychert et al. 2018). We do not view the olivine compositions as a direct proxy for LAB depth (as done in, e.g. Matzen et al. 2017a), but consider the SEVZ high-Ni olivines as the crystallization products of deep accumulated melts that avoided mixing and equilibration at the top of the melting column in the mantle (which may or may not correspond to LAB). This view is supported by (1) the previously discussed mantle melt mixing trend in Brattaskjól and Hvammsmúli olivine populations, where the high-Ni olivines represent a deep endmember in the presence of apparent shallower mantle melt; and (2) the likelihood of mantle-melt equilibration pressures greater than 2 GPa supported by the evidence for deep olivine crystallization and "garnet signature" (low Sc) in olivine crystals. Essentially, the SEVZ high-Ni/low-Mn olivines are an indication of the survival of mantle melts from the deep parts of the mantle-melting column to the *T*–*P*-conditions of olivine crystallization.

What makes SEVZ special?

High-Ni, low-Mn olivines seem to be characteristic for SEVZ but absent in SVZ and the rift-zone magmas. This is noteworthy, especially regarding the trace element enriched SVZ lavas (e.g. Berserkjahraun), which, alike SEVZ lavas, have compositional and isotopic characteristics arguing in favor of melt extraction from relatively deep in the mantle (e.g. Kokfelt et al. 2006). Why the apparent signature of deep mantle melting in olivines at SEVZ in particular?

It is likely that deep mantle melts are in fact ubiquitous in all rift-zones and off-rift zones in Iceland, but they are usually diluted by melt mixing in the mantle or mid–lower-crust (Maclennan 2008a; Neave et al. 2013). Although magmas originating from deep portions of the mantle can erupt at the rift zones (as indicated by trace element enriched lavas like Stapafell and Gaesafjöll, Shorttle and Maclennan 2011), survival of deep melts is most likely to occur at off-rift settings, like at SEVZ, where the degree of mantle melting is low (Kokfelt et al. 2006). Furthermore, as magmatism at SEVZ is a relatively recent phenomenon (younger than 3 Ma, Martin et al. 2011), the underlying mantle may have not yet been depleted of the most fusible lithologies (e.g. KG2), which further biases the melt production to increased depth. Sufficiently refractory shallow mantle (e.g. harzburgite, Shorttle

et al. 2014) and effective vertical melt transport could also inhibit melt mixing in the mantle and promote magma derivation from depth. Channelized melt transport (Spiegelman and Kelemen 2003; Weatherley and Katz 2012; Rudge et al. 2013), in contrast to melt extraction by diffuse (equilibrium) porous flow (Lundstrom et al. 1995; Niu 1997; Dijkstra et al. 2003), may be the required melt transfer mechanism for survival of deep mantle melts and potentially important in the mantle below SEVZ.

The nature of the crustal magma plumbing systems beneath Eyjafjallajökull and Vestmannaeyjar is also likely to contribute to the crystallization, and survival, of high-Ni/low-Mn olivine macrocrysts. Even if a parcel of deep mantle melt were to keep its coherency during transit through the mantle and manage to crystallize equilibrium olivine in the crust (with high-Ni, low-Mn), this olivine would need to be erupted relatively fast to avoid re-equilibration with accumulated magmas with diverse composition during storage in the crust or uppermost mantle. Olivine macrocrysts in Iceland are rarely in equilibrium with their carrier melts, and are prone to be modified by diffusive re-equilibration (Thomson and Maclennan 2013). For example, if the Hvammsmúli and Brattaskjól olivine population (Fig. 8) had resided in a magma reservoir for extended time, the compositional signature of deep origin would have been erased. The originally heterogeneous olivine cargo (high variability in Ni, Mn and Ca in high-Fo olivines; Fig. 8) would have re-equilibrated diffusively with itself and the carrier magma, suppressing extremes in Ni, Mn and Ca. In the end, homogenized olivine population would have only modest enrichment in Fe/Mn and "Kistufell-like" Ni and Ca (Fig. 6) and the original subpopulation of high-Ni olivines might only be identifiable from olivine-hosted melt inclusions or slowly diffusing trace elements.

There are indications of short-lived and poorly developed deep magma storage systems below Eyjafjallajökull and Vestmannaeyjar. U-series disequilibria (Sigmarsson 1996) and absence of equilibrium phenocryst assemblages (Mattsson and Oskarsson 2005) in Vestmannaeyjar lavas suggest rapid differentiation within a deep and cold crust and short magmatic residence times. Furthermore, deep seismicity prior to and during the Eyjafjallajökull 2010 eruption suggests near-direct magma derivation from the mantle (Tarasewicz et al. 2012). Relatively fast transport of mantle melts limits crystal–melt equilibration and magma mixing, promoting survival of compositional extremes in the mineral cargo. Rather little is known about the lower-crustal magma storage zones in SVZ, but the maturity of SVZ volcanism could hint at well-established magma reservoirs. SVZ low-degree primitive magmas may reside in the deep crust (or shallow mantle) long enough that magmas aggregated from different depths in the mantle melting column are better mixed and equilibrated. This limits compositional variability in populations of primitive olivine, and suppresses a potential "deep melting signature" (high-Ni/low-Mn in olivines).

Conclusion

In each of the sampling locations, major and trace element trends in olivine populations reflect events of fractional crystallization, magma mixing and diffusive re-equilibration. Two Eyjafjallajökull transitional basalts also show large variability in the Ni, Mn and Ca contents of primitive $Fo_{88.2–89.6}$ olivines, which we consider as a mixing trend of melts equilibrated at different levels in the mantle. Eyjafjallajökull and Vestmannaeyjar volcanic systems in SEVZ have anomalous (high-Ni and Fe/Mn-enriched) olivines compared to previously published olivine data from Iceland. These olivine macrocrysts likely crystallized from magmas that equilibrated with the mantle at relatively high temperatures and pressures, at depths of > 45 km and possibly as deep as 66–81 km near the spinel-garnet peridotite transition. The evidence for deep mantle melts that avoided mixing and kept their coherency while migrating up through the upper mantle and the crust is an indication of effective vertical magma transport below SEVZ.

Acknowledgements Open access funding provided by University of Helsinki including Helsinki University Central Hospital. We thank Matthew Pankhurst and Sæmundur Ari Halldórsson for providing the Eyjafjallajökull 2010 and Berserkjahraun samples, respectively. Maren Kahl is thanked for discussions and Atli Hjartarson for skillfully preparing the samples for microprobe and LA–ICP–MS analyses. Comments from two anonymous reviewers improved the manuscript. This work was funded by the Nordic Volcanological Center, Icelandic Research Fund doctoral student Grant (185267-051) and Landsvirkjun geothermal research grant.

References

Allègre CJ, Turcotte DL (1986) Implications of a two-component marble-cake mantle. Nature. https://doi.org/10.1038/323123a0

Árnadóttir T, Lund B, Jiang W et al (2009) Glacial rebound and plate spreading: results from the first countrywide GPS observations in Iceland. Geophys J Int 177:691–716. https://doi.org/10.1111/j.1365-246X.2008.04059.x

Asimow PD, Hirschmann MM, Ghiorso MS et al (1995) The effect of pressure-induced solid-solid phase transitions on decompression melting of the mantle. Geochim Cosmochim Acta 59:4489–4506. https://doi.org/10.1016/0016-7037(95)00252-U

Balta JB, Asimow PD, Mosenfelder JL (2011) Manganese partitioning during hydrous melting of peridotite. Geochim Cosmochim Acta 75:5819–5833. https://doi.org/10.1016/j.gca.2011.05.026

Barnhoorn A, van der Wal W, Drury MR (2011) Upper mantle viscosity and lithospheric thickness under Iceland. J Geodyn 52:260–270. https://doi.org/10.1016/j.jog.2011.01.002

Batanova VG, Sobolev AV, Kuzmin DV (2015) Trace element analysis of olivine: high precision analytical method for JEOL JXA-8230 electron probe microanalyser. Chem Geol 419:149–157. https://doi.org/10.1016/j.chemgeo.2015.10.042

Beattie P, Ford C, Russell D (1991) Partition coefficients for olivine-melt and ortho-pyroxene-melt systems. Contrib Miner Pet 109:212–224. https://doi.org/10.1007/bf00306480

Berman RG, Koziol AM (1991) Ternary excess properties of grossular-pyrope-almandine garnet and their influence in geothermobarometry. Am Mineral 76:1223–1231

Bjarnason IT, Schmeling H (2009) The lithosphere and asthenosphere of the Iceland hotspot from surface waves. Geophys J Int. https://doi.org/10.1111/j.1365-246X.2009.04155.x

Breddam K (2002) Kistufell: primitive melt from the Iceland mantle plume. J Petrol 43:345–373. https://doi.org/10.1093/petrology/43.2.345

Breddam K, Kurz MD, Storey M (2000) Mapping out the conduit of the Iceland mantle plume with helium isotopes. Earth Planet Sci Lett 176:45–55. https://doi.org/10.1016/S0012-821X(99)00313-1

Brown EL, Lesher CE (2014) North Atlantic magmatism controlled by temperature, mantle composition and buoyancy. Nat Geosci 7:820–824. https://doi.org/10.1038/ngeo2264

Canil D (1997) Vanadium partitioning and the oxidation state of Archaean komatiite magmas. Nature 389:842–845. https://doi.org/10.1038/39860

Chauvel C, Hémond C (2000) Melting of a complete section of recycled oceanic crust: trace element and Pb isotopic evidence from Iceland. Geochem Geophys Geosyst 1:1–22. https://doi.org/10.1029/1999GC000002

Chauvel C, Lewin E, Carpentier M et al (2008) Role of recycled oceanic basalt and sediment in generating the Hf-Nd mantle array. Nat Geosci. https://doi.org/10.1038/ngeo.2007.51

Costa F, Morgan D (2010) Time constraints from chemical equilibration in magmatic crystals. Timescales of magmatic processes: from core to atmosphere. Wiley, Chichester, pp 125–159

Darbyshire FA, White RS, Priestley KF (2000) Structure of the crust and uppermost mantle of Iceland from a combined seismic and gravity study. Earth Planet Sci Lett 181:409–428. https://doi.org/10.1016/S0012-821X(00)00206-5

Davis FA, Humayun M, Hirschmann MM, Cooper RS (2013) Experimentally determined mineral/melt partitioning of first-row transition elements (FRTE) during partial melting of peridotite at 3 GPa. Geochim Cosmochim Acta 104:232–260. https://doi.org/10.1016/j.gca.2012.11.009

Dijkstra AH, Barth MG, Drury MR et al (2003) Diffuse porous melt flow and melt-rock reaction in the mantle lithosphere at a slow-spreading ridge: a structural petrology and LA–ICP–MS study of the Othris Peridotite Massif (Greece). Geochem Geophys Geosyst. https://doi.org/10.1029/2001GC000278

Dohmen R, Becker HW, Chakraborty S (2007) Fe-Mg diffusion in olivine I: experimental determination between 700 and 1200 °C as a function of composition, crystal orientation and oxygen fugacity. Phys Chem Miner 34:389–407. https://doi.org/10.1007/s00269-007-0157-7

Fedorova T, Jacoby WR, Wallner H (2005) Crust-mantle transition and Moho model for Iceland and surroundings from seismic, topography, and gravity data. Tectonophysics 396:119–140. https://doi.org/10.1016/j.tecto.2004.11.004

Fitton J, Saunders A, Norry M et al (1997) Thermal and chemical structure of the Iceland plume. Earth Planet Sci Lett Planet Sci Lett 153:197–208. https://doi.org/10.1016/S0012-821X(97)00170-2

Fitton JG, Saunders AD, Kempton PD, Hardarson BS (2003) Does depleted mantle form an intrinsic part of the Iceland plume? Geochem Geophys Geosyst. https://doi.org/10.1029/2002GC000424

Furman T, Frey FA, Park KH (1991) Chemical constraints on the petrogenesis of mildly alkaline lavas from Vestmannaeyjar, Iceland: the Eldfell (1973) and Surtsey (1963–1967) eruptions. Contrib Mineral Petrol 109:19–37. https://doi.org/10.1007/BF00687198

Ghiorso MS, Hirschmann MM, Reiners PW, Kress VC (2002) The pMELTS: a revision of MELTS for improved calculation of phase relations and major element partitioning related to partial melting of the mantle to 3 GPa. Geochem Geophys Geosyst 3:1–35. https://doi.org/10.1029/2001GC000217

Green DH, Ringwood AE (1963) Mineral assemblages in a model mantle composition. J Geophys Res. https://doi.org/10.1029/JZ068i003p00937

Green PJ, Seheult AH, Silverman BW (1988) Density estimation for statistics and data analysis. Appl Stat 37:120. https://doi.org/10.2307/2347507

Guillong M, Meier DL, Allan MM et al (2008) SILLS: a Matlab-based program for the reduction of laser ablation ICP–MS data of homogeneous materials and inclusions. Mineral Assoc Can Short Course 40:328–333

Gurenko AA, Hoernle KA, Sobolev AV et al (2010) Source components of the Gran Canaria (Canary Islands) shield stage magmas: evidence from olivine composition and Sr–Nd–Pb isotopes. Contrib Mineral Petrol 159:689–702. https://doi.org/10.1007/s00410-009-0448-8

Hardarson BS, Fitton JG, Ellam RM, Pringle MS (1997) Rift relocation—a geochemical and geochronological investigation of a palaeo-rift in northwest Iceland. Earth Planet Sci Lett 153:181–196. https://doi.org/10.1016/S0012-821X(97)00145-3

Hauri EH (1996) Major-element variability in the Hawaiian mantle plume. Nature 382:415–419. https://doi.org/10.1038/382415a0

Heinonen JS, Fusswinkel T (2017) High Ni and low Mn/Fe in olivine phenocrysts of the Karoo meimechites do not reflect pyroxenitic mantle sources. Chem Geol 467:134–142. https://doi.org/10.1016/j.chemgeo.2017.08.002

Hemond C, Arndt NT, Lichtenstein U et al (1993) The heterogeneous Iceland plume: Nd-Sr-O isotopes and trace element constraints. J Geophys Res 98:15833. https://doi.org/10.1029/93JB01093

Herzberg C (2011) Identification of source lithology in the Hawaiian and Canary islands: implications for origins. J Petrol 52:113–146. https://doi.org/10.1093/petrology/egq075

Herzberg CT, Asimow PD (2015) PRIMELT3 MEGA.XLSM software for primarymagma calculation: peridotite primarymagma MgO contents fromthe liquidus to the solidus. Geochem Geophys Geosyst 16:563–578. https://doi.org/10.1002/2014GC005631.Received

Herzberg C, O'Hara MJ (2002) Plume-associated ultramafic magmas of phanerozoic age. J Petrol 43:1857–1883. https://doi.org/10.1093/petrology/43.10.1857

Herzberg C, Asimow PD, Ionov DA et al (2013) Nickel and helium evidence for melt above the core-mantle boundary. Nature 493:393–397. https://doi.org/10.1038/nature11771

Herzberg C, Cabral RA, Jackson MG et al (2014) Phantom Archean crust in Mangaia hotspot lavas and the meaning of heterogeneous mantle. Earth Planet Sci Lett 396:97–106. https://doi.org/10.1016/j.epsl.2014.03.065

Herzberg CT, Vidito C, Starkey NA et al (2016) Nickel-cobalt contents of olivine record origins of mantle peridotite and related rocks. Am Mineral 101:1952–1966. https://doi.org/10.2138/am-2016-5538

Hirose K, Kushiro I (1993) Partial melting of dry peridotites at high pressures: determination of compositions of melts segregated from peridotite using aggregates of diamond. Earth Planet Sci

Lett 114:477–489. https://doi.org/10.1016/0012-821X(93)90077-M
Hofmann AW, White WM (1982) Mantle plumes from ancient oceanic crust. Earth Planet Sci Lett 57:421–436. https://doi.org/10.1016/0012-821X(82)90161-3
Hole MJ (2018) Mineralogical and geochemical evidence for polybaric fractional crystallization of continental flood basalts and implications for identification of peridotite and pyroxenite source lithologies. Earth-Sci Rev 176:51–67. https://doi.org/10.1016/j.earscirev.2017.09.014
Jakobsson SP (1968) The geology and petrography of the Vestmann Islands: a preliminary report. Surtsey Res Prog Rep 4:113–129
Jakobsson SP (1972) Chemistry and distribution pattern of recent basaltic rocks in Iceland. Lithos 5:365–386. https://doi.org/10.1016/0024-4937(72)90090-4
Jakobsson SP (1979) Petrology of recent basalts of the Eastern Volcanic zone. Acta Nat alia Islandica, Iceland
Jakobsson SP, Pedersen AK, Rönsbo JG, Melchior Larsen L (1973) Petrology of mugearite-hawaiite: early extrusives in the 1973 Heimaey eruption, Iceland. Lithos 6:203–214. https://doi.org/10.1016/0024-4937(73)90065-0
Jakobsson SP, Jonasson K, Sigurdsson IA (2008) The three igneous rock series of Iceland. Jökull 58:117–138
Jenkins J, Maclennan J, Green RG et al (2018) Crustal formation on a spreading ridge above a mantle plume: receiver function imaging of the Icelandic crust. J Geophys Res Solid Earth 123:5190–5208. https://doi.org/10.1029/2017JB015121
Jennings ES, Holland TJB (2015) A simple thermodynamic model for melting of peridotite in the system NCFMASOCr. J Petrol 56:869–892. https://doi.org/10.1093/petrology/egv020
Jennings ES, Gibson SA, Maclennan J, Heinonen JS (2017) Deep mixing of mantle melts beneath continental flood basalt provinces: constraints from olivine-hosted melt inclusions in primitive magmas. Geochim Cosmochim Acta 196:36–57. https://doi.org/10.1016/j.gca.2016.09.015
Jochum KP, Nohl U, Herwig K et al (2005) GeoReM: a new geochemical database for reference materials and isotopic standards. Geostand Geoanal Res 29:333–338. https://doi.org/10.1111/j.1751-908X.2005.tb00904.x
Jóhannesson H (1994) Geological map of Iceland, sheet 2, 1:250 000. West-Iceland, 2nd edn. Icelandic Meseum of Natural History and Iceland Geodetic Survey, Reykjavik
Keiding JK, Sigmarsson O (2012) Geothermobarometry of the 2010 Eyjafjallajökull eruption: new constraints on Icelandic magma plumbing systems. J Geophys Res Solid Earth 117:1–15. https://doi.org/10.1029/2011JB008829
Kogiso T, Hirose K, Takahashi E (1998) Melting experiments on homogeneous mixtures of peridotite and basalt: application to the genesis of ocean island basalts. Earth Planet Sci Lett 162:45–61. https://doi.org/10.1016/S0012-821X(98)00156-3
Kokfelt TF, Hoernle K, Hauff F et al (2006) Combined trace element and Pb–Nd–Sr–O isotope evidence for recycled oceanic crust (upper and lower) in the Iceland mantle plume. J Petrol 47:1705–1749. https://doi.org/10.1093/petrology/egl025
Lambart S (2017) No direct contribution of recycled crust in Icelandic basalts. Geochem Perspect Lett. https://doi.org/10.7185/geochemlet.1728
Lambart S, Laporte D, Provost A, Schiano P (2012) Fate of pyroxenite-derived melts in the peridotitic mantle: thermodynamic and experimental constraints. J Petrol 53:451–476. https://doi.org/10.1093/petrology/egr068
Lambart S, Baker MB, Stolper EM (2016) The role of pyroxenite in basalt genesis: melt-PX, a melting parameterization for mantle pyroxenites between 0.9 and 5 GPa. J Geophys Res Solid Earth 121:5708–5735. https://doi.org/10.1002/2015JB012762
Laubier M, Grove TL, Langmuir CH et al (2014) Trace element mineral/melt partitioning for basaltic and basaltic andesitic melts: an experimental and laser ICP-MS study with application to the oxidation state of mantle source regions. Earth Planet Sci Lett 392:265–278. https://doi.org/10.1016/j.epsl.2014.01.053
Le Roux V, Lee CT, Turner SJ (2010) Zn/Fe systematics in mafic and ultramafic systems: implications for detecting major element heterogeneities in the Earth's mantle. Geochim Cosmochim Acta 74:2779–2796. https://doi.org/10.1016/j.gca.2010.02.004
Le Roux V, Dasgupta R, Lee CT (2011) Mineralogical heterogeneities in the Earth's mantle: constraints from Mn Co, Ni and Zn partitioning during partial melting. Earth Planet Sci Lett 307:395–408. https://doi.org/10.1016/j.epsl.2011.05.014
Lee CT, Luffi P, Chin EJ et al (2012) Copper systematics in arc magmas and implications for crust-mantle differentiation. Science 336:64–68. https://doi.org/10.1126/science.1217313
Li C, Ripley EM (2010) The relative effects of composition and temperature on olivine-liquid Ni partitioning: statistical deconvolution and implications for petrologic modeling. Chem Geol 275:99–104. https://doi.org/10.1016/j.chemgeo.2010.05.001
Loughlin SC (1995) The evolution of the Eyjafjöll volcanic system, southern Iceland. Ph.D. thesis, p 319, University of Durham, Durham, UK
Lundstrom CC, Gill J, Williams Q, Perfit MR (1995) Mantle melting and basalt extraction by equilibrium porous flow. Science 270:1958–1961. https://doi.org/10.1126/science.270.5244.1958
Lynn KJ, Shea T, Garcia MO (2017) Nickel variability in Hawaiian olivine: evaluating the relative contributions from mantle and crustal processes. Am Mineral 102:507–518. https://doi.org/10.2138/am-2017-5763
Maclennan J (2008a) Concurrent mixing and cooling of melts under Iceland. J Petrol 49:1931–1953. https://doi.org/10.1093/petrology/egn052
Maclennan J (2008b) Lead isotope variability in olivine-hosted melt inclusions from Iceland. Geochim Cosmochim Acta 72:4159–4176. https://doi.org/10.1016/j.gca.2008.05.034
Martin E, Paquette JL, Bosse V et al (2011) Geodynamics of rift–plume interaction in Iceland as constrained by new 40Ar/39Ar and in situ U-Pb zircon ages. Earth Planet Sci Lett 311:28–38. https://doi.org/10.1016/j.epsl.2011.08.036
Matthews S, Shorttle O, Maclennan J (2016) The temperature of the Icelandic mantle from olivine-spinel aluminum exchange thermometry. Geochem Geophys Geosyst. https://doi.org/10.1002/2016GC006497
Mattsson H, Höskuldsson Á (2003) Geology of the Heimaey volcanic centre, south Iceland: early evolution of a central volcano in a propagating rift? J Volcanol Geotherm Res 127:55–71. https://doi.org/10.1016/S0377-0273(03)00178-1
Mattsson HB, Oskarsson N (2005) Petrogenesis of alkaline basalts at the tip of a propagating rift: evidence from the Heimaey volcanic centre, south Iceland. J Volcanol Geotherm Res 147:245–267. https://doi.org/10.1016/j.jvolgeores.2005.04.004
Matzen AK, Baker MB, Beckett JR, Stolper EM (2013) The temperature and pressure dependence of nickel partitioning between olivine and silicate melt. J Petrol 54:2521–2545. https://doi.org/10.1093/petrology/egt055
Matzen AK, Baker MB, Beckett JR et al (2017a) The effect of liquid composition on the partitioning of Ni between olivine and silicate melt. Contrib Mineral Petrol 172:3. https://doi.org/10.1007/s00410-016-1319-8
Matzen AK, Wood BJ, Baker MB, Stolper EM (2017b) The roles of pyroxenite and peridotite in the mantle sources of oceanic basalts. Nat Geosci 10:530–535. https://doi.org/10.1038/ngeo2968
Neave DA, Passmore E, Maclennan J et al (2013) Crystal–melt relationships and the record of deep mixing and crystallization in the

ad 1783 laki eruption, Iceland. J Petrol 54:1661–1690. https://doi.org/10.1093/petrology/egt027
Neave DA, Shorttle O, Oeser M et al (2018) Mantle-derived trace element variability in olivines and their melt inclusions. Earth Planet Sci Lett 483:90–104. https://doi.org/10.1016/j.epsl.2017.12.014
Niu Y (1997) Mantle melting and melt extraction processes beneath ocean ridges: evidence from abyssal peridotites. J Petrol 38:1047–1074. https://doi.org/10.1093/petroj/38.8.1047
Niu Y, Wilson M, Humphreys ER, O'Hara MJ (2011) The origin of intra-plate ocean island basalts (OIB): the lid effect and its geodynamic implications. J Petrol 52:1443–1468. https://doi.org/10.1093/petrology/egr030
O'Hara MJ (1968) The bearing of phase equilibria studies in synthetic and natural systems on the origin and evolution of basic and ultrabasic rocks. Earth-Sci Rev. https://doi.org/10.1016/0012-8252(68)90147-5
Pagli C, Sigmundsson F, Lund B et al (2007) Glacio-isostatic deformation around the Vatnajökull ice cap, Iceland, induced by recent climate warming: GPS observations and finite element modeling. J Geophys Res Solid Earth 112:1–12. https://doi.org/10.1029/2006JB004421
Pankhurst MJ, Morgan DJ, Thordarson T, Loughlin SC (2018) Magmatic crystal records in time, space, and process, causatively linked with volcanic unrest. Earth Planet Sci Lett 493:231–241. https://doi.org/10.1016/j.epsl.2018.04.025
Peate DW, Baker JA, Jakobsson SP et al (2009) Historic magmatism on the Reykjanes Peninsula, Iceland: a snap-shot of melt generation at a ridge segment. Contrib Mineral Petrol 157:359–382. https://doi.org/10.1007/s00410-008-0339-4
Peate DW, Breddam K, Baker JA et al (2010) Compositional characteristics and spatial distribution of enriched Icelandic mantle components. J Petrol 51:1447–1475. https://doi.org/10.1093/petrology/egq025
Putirka K, Ryerson FJ, Perfit M, Ridley WI (2011) Mineralogy and composition of the oceanic mantle. J Petrol 52:279–313. https://doi.org/10.1093/petrology/egq080
Putirka K, Tao Y, Hari KR et al (2018) The mantle source of thermal plumes: trace and minor elements in olivine and major oxides of primitive liquids (and why the olivine compositions don't matter). Am Mineral 103:1253–1270. https://doi.org/10.2138/am-2018-6192
Rudge JF, Maclennan J, Stracke A (2013) The geochemical consequences of mixing melts from a heterogeneous mantle. Geochim Cosmochim Acta 114:112–143. https://doi.org/10.1016/j.gca.2013.03.042
Ryan JG, Langmuir CH (1987) The systematics of lithium abundances in young volcanic rocks. Geochim Cosmochim Acta 51:1727–1741. https://doi.org/10.1016/0016-7037(87)90351-6
Rychert CA, Harmon N, Armitage JJ (2018) Seismic imaging of thickened lithosphere resulting from plume pulsing beneath Iceland. Geochem Geophys Geosyst 19:1789–1799. https://doi.org/10.1029/2018GC007501
Sæmundsson K (1979) Outline of the geology of Iceland. Jökull 29:11–28
Sæmundsson K (1995) Svartsengi geological map (bedrock) 1:25,000. Orkustofnun, Hitaveita Sudurnesja and Landmaelingar Islands, Reykjavik
Sæmundsson K, Jóhannesson H, Hjartarson Á et al (2010) Geological map of Southewest Iceland. Icel Geosurv 1:100000
Shorttle O, Maclennan J (2011) Compositional trends of Icelandic basalts: implications for short-length scale lithological heterogeneity in mantle plumes. Geochem Geophys Geosyst. https://doi.org/10.1029/2011GC003748
Shorttle O, Maclennan J, Lambart S (2014) Quantifying lithological variability in the mantle. Earth Planet Sci Lett 395:24–40. https://doi.org/10.1016/j.epsl.2014.03.040
Sigmarsson O (1996) Short magma chamber residence time at an Icelandic volcano inferred from U-series disequilibria. Nature 382:440–442. https://doi.org/10.1038/382440a0
Sigmarsson O, Vlastelic I, Andreasen R et al (2011) Remobilization of silicic intrusion by mafic magmas during the 2010 Eyjafjallajökull eruption. Solid Earth 2:271–281. https://doi.org/10.5194/se-2-271-2011
Smith PM, Asimow PD (2005) Adiabat-1ph: a new public front-end to the MELTS, pMELTS, and pHMELTS models. Geochem Geophys Geosyst 6:1–8. https://doi.org/10.1029/2004GC000816
Sobolev AV, Hofmann AW, Sobolev SV, Nikogosian IK (2005) An olivine-free mantle source of Hawaiian shield basalts. Nature 434:590–597. https://doi.org/10.1038/nature03411
Sobolev AV, Hofmann AW, Kuzmin DV et al (2007) The amount of recycled crust in sources of mantle-derived melts. Science 316:412–417. https://doi.org/10.1126/science.1138113
Sobolev AV, Hofmann AW, Brügmann G et al (2008) A quantitative link between recycling and osmium isotopes. Science 321:536. https://doi.org/10.1126/science.1158452
Spandler C, Pettke T, Rubatto D (2011) Internal and external fluid sources for eclogite-facies veins in the Monviso Meta-ophiolite, Western Alps: implications for fluid flow in subduction zones. J Petrol 52:1207–1236. https://doi.org/10.1093/petrology/egr025
Spice HE, Fitton JG, Kirstein LA (2016) Temperature fluctuation of the Iceland mantle plume through time. Geochem Geophys Geosyst. https://doi.org/10.1002/2015GC006059
Spiegelman M, Kelemen PB (2003) Extreme chemical variability as a consequence of channelized melt transport. Geochem Geophys Geosyst. https://doi.org/10.1029/2002GC000336
Sugawara T (2000) Empirical relationships between temperature, pressure, and MgO content in olivine and pyroxene saturated liquid. J Geophys Res 105:8457. https://doi.org/10.1029/2000JB900010
Tarasewicz J, Brandsdóttir B, White RS et al (2012) Using microearthquakes to track repeated magma intrusions beneath the Eyjafjallajökull stratovolcano, Iceland. J Geophys Res Solid Earth 117:1–13. https://doi.org/10.1029/2011JB008751
Thirlwall MF, Gee MAM, Taylor RN, Murton BJ (2004) Mantle components in Iceland and adjacent ridges investigated using double-spike Pb isotope ratios. Geochim Cosmochim Acta 68:361–386. https://doi.org/10.1016/S0016-7037(03)00424-1
Thirlwall MF, Gee MAM, Lowry D et al (2006) Low δ18O in the Icelandic mantle and its origins: evidence from Reykjanes Ridge and Icelandic lavas. Geochim Cosmochim Acta 70:993–1019. https://doi.org/10.1016/j.gca.2005.09.008
Thomson A, Maclennan J (2013) The distribution of olivine compositions in icelandic basalts and picrites. J Petrol 54:745–768. https://doi.org/10.1093/petrology/egs083
Thordarson T, Larsen G (2007) Volcanism in Iceland in historical time: volcano types, eruption styles and eruptive history. J Geodyn 43:118–152. https://doi.org/10.1016/j.jog.2006.09.005
Trela J, Vidito C, Gazel E et al (2015) Recycled crust in the galápagos plume source at 70 ma: implications for plume evolution. Earth Planet Sci Lett 425:268–277. https://doi.org/10.1016/j.epsl.2015.05.036
Viccaro M, Giuffrida M, Nicotra E, Cristofolini R (2016) Timescales of magma storage and migration recorded by olivine crystals in basalts of the March–April 2010 eruption at Eyjafjallajökull volcano, Iceland. Am Mineral 101:222–230. https://doi.org/10.2138/am-2016-5365
Wang Z, Gaetani GA (2008) Partitioning of Ni between olivine and siliceous eclogite partial melt: experimental constraints on

the mantle source of Hawaiian basalts. Contrib Mineral Petrol 156:661–678. https://doi.org/10.1007/s00410-008-0308-y

Weatherley SM, Katz RF (2012) Melting and channelized magmatic flow in chemically heterogeneous, upwelling mantle. Geochem Geophys Geosyst. https://doi.org/10.1029/2011GC003989

Wiese PK (1992) Geochemistry and geochronology of the Eyjafjoll volcanic system. Unpublished MSc Thesis, University of Oregon

Wolfe CJ, Bjarnason IT, VanDecar JC, Solomon SC (1997) Seismic structure of the Iceland mantle plume. Nature 385:245–247. https://doi.org/10.1038/385245a0